Journal of Advanced Ceramics
先进陶瓷
ISSN 2226-4108
CN 10-1154/TQ
清華大学出版社 Tsinghua University Press
SciOpen

J Adv Ceram 2026, **15**: 9221329

https://doi.org/10.26599/JAC.2026.9221329

Research Article

Calcium zinc oxysulfide: Newfound polytypes for potential optoelectronic applications

Dejan Zagorac[1,2,*], Matej Fonović[3], Branko Matović[1,2], Marjan Ranđelović[4], Svetlana Butulija[2], Elena Raksha[5], Jelena Zagorac[1,2]

[1] *Center of Excellence „Center for Synthesis, Processing and Characterization of Materials for Application in Extreme Conditions - Cextreme Lab“, Belgrade, Serbia;*
[2] *Department of Material Science, Vinča Institute of Nuclear Sciences - National Institute of the Republic of Serbia, University of Belgrade, Belgrade, Serbia;*
[3] *University of Rijeka, Faculty of Engineering, Rijeka, Croatia;*
[4] *Department of Chemistry, Faculty of Mathematics and Natural Sciences, University of Niš, 18000 Niš, Serbia;*
[5] *Frank Laboratory of Neutron Physics, Joint Institute for Nuclear Research, Dubna, Russia*

*Corresponding author:

E-mail: dzagorac@vinca.rs

Received: February 3, 2026; Revised: May 22, 2026; Accepted: June 2, 2026

Abstract: CaZnOS has attracted significant scientific interest, particularly for its layered structure, advanced properties, outstanding doping ability, and structure-property relationships. The CaZnOS compound has been synthesized through high-temperature experiments and characterized by X-ray powder diffraction (XRPD). The crystal structure of CaZnOS exhibits non-centrosymmetric hexagonal symmetry with the space group $P6_3mc$. The spectrum of possible CaZnOS polytypes has been investigated, predicting structural configurations that differ from those previously proposed or observed in CaZnOS, encompassing bulk crystal forms, nanostructures, or junction-based architectures. All computations were conducted from first principles utilizing density functional theory (DFT) and five different functionals (LDA−PZ, GGA−PBE, B3LYP, PBE0, and HSE06). Recently developed algorithms were used for structure prediction, and the predicted CaZnOS polytypes were investigated for their stability, electronic, and vibrational properties. Consequently, numerous potential stable and metastable CaZnOS polytypes have been identified, opening new possibilities for the synthesis of innovative materials with improved properties.

Keywords: CaZnOS, XRD, DFT, Luminescent semiconductor; polytypes; heterostructures.

1. Introduction

Persistent luminescence materials, also referred to as afterglow materials or long-lasting phosphors, are distinguished by their capacity to store energy from excitation sources such as ultraviolet, visible, or X-ray radiation, and to subsequently release this energy as visible or near-infrared light over extended periods ranging from several minutes to several days after the excitation ceases. [1-3] The mechanism is based on the presence of charge-carrier traps, which may arise from internal structural defects or intentionally introduced impurity levels within the band gap. Upon excitation, these traps capture and store electrons or holes. Subsequently, the stored energy is gradually released at room temperature via thermal stimulation, leading to charge-carrier recombination and delayed light emission. [4, 5] The advanced applications of these materials span a diverse range of fields, from safety lighting and photovoltaics to sensing devices, biomedical imaging, display technologies, and security applications. [6-10] The primary categories of luminescent materials are represented by several well-defined chemical systems. These include alkaline earth aluminates (e.g., $SrAl_2O_4$ doped with Eu^{2+} or Dy^{3+}) [11, 12], along with various silicates and oxysulfides such as CaZnOS and $Sr_2MgSi_2O_7$. [13, 14] In addition, important classes comprise nitrides and oxynitrides, represented by compounds such as $CaAlSiN_3$ and $SrSi_2O_2N_2$. [15, 16]. Beyond these established categories, newer systems based on rare-earth-doped gallates, fluorides, and phosphates are also the subject of active research. [17-20] A comparison of well-known persistent luminescence materials, including their emission properties and main applications, is presented in Table 1.

Table 1. Overview of some well-known persistent luminescence materials with their properties.

Chemical system	Typical dopant	Emission color	Afterglow duration	Application
$ZnGa_2O_4$ [12]	Cr^{3+}	Near–Infrared light	Hours to days	Bio-imaging
$CaAl_2O_4$ [21]	Eu^{2+}, Nd^{3+}	Blue	Hours	Luminescent coatings
Y_2O_2S [22]	Eu^{3+}	Red/green	Minutes	Display phosphorus

$SrAl_2O_4$ [23]	Eu^{2+}, Dy^{3+}	Green	Hours	Safety signs
ZrO_2, TiO_2 [24]	Rare earth metals	UV–Visible	Variable	Photocatalysis
$LaAlO_3$ [25]	Cr^{3+}, Nd^{3+}	Near-Infrared light	Hours	Anti-counterfeiting
CaZnOS [13]	Eu^{2+}	Green–blue	Minutes to hours	LED phosphors
$Sr_4Al_{14}O_{25}$ [26]	Eu^{2+}, Eu^{3+}	Blue–green	Hours	Emergency signage
$Sr_2MgSi_2O_7$ [14]	Eu^{2+}, Dy^{3+}	Blue	Hours	Decorative paints

CaZnOS has attracted considerable scientific attention for a long time. Over the years, various doping strategies have been widely investigated to precisely tune their optical and electronic properties, enabling control over emission wavelength, intensity, and energy transfer processes. As reported in Ref. [27], effective lanthanide-doping strategies were developed to incorporate a wide range of lanthanide ions into the CaZnOS matrix, achieving tunable mechanoluminescence spanning violet to near-infrared wavelengths. Another study on CaZnOS crystals doped with Cu^{+}, Pb^{2+}, Bi^{3+}, Sb^{3+}, Mn^{2+}, and various rare-earth (RE^{3+}) ions demonstrated that combinatorial doping provides a strategy for independently controlling both the activator–trap system and the trap-filling mechanisms within a single persistent luminescence phosphor. This approach allows fine-tuning of the material's luminescent properties, thereby enhancing afterglow performance and tailoring emission characteristics for specific applications. [28]

A team of researchers developed a novel approach to synthesize the red-emitting phosphor CaZnOS: Eu^{2+} from $CaCO_3$, ZnS, Eu_2O_3, and $CeCl_3$ via controlled sintering. They found that Ce^{3+} ions can act as a reducing agent, facilitating the formation of Eu^{2+} within the CaZnOS matrix under an inert atmosphere. [29] In another investigation, the optical properties and radiative recombination kinetics of pure CaZnOS were explored under both intrinsic and extrinsic excitation. The vibrational characteristics, obtained via Raman spectroscopy and supported by DFT calculations, revealed 10 Raman-active modes in a crystal structure corresponding to the $P6_3mc$ ($C4_6v$) space group. [30] A recent work reported the successful synthesis of CaZnOS samples doped with varying concentrations of Mn^{2+} ions. For the first time, this work demonstrated the near-infrared mechanoluminescence of Mn^{2+}-doped CaZnOS. Owing to its exceptional luminescent properties and notable chemical stability, CaZnOS is a highly promising candidate for a range of advanced applications. This combination of attributes underscores its significant potential for the development of new optoelectronic, photocatalytic, and phosphorescent materials. Finally, the relative abundance and chemical stability of calcium, zinc, oxygen, and sulfur render CaZnOS a highly promising candidate for both fundamental studies and a wide range of practical technological applications.

The present theoretical exploration of the CaZnOS landscape has revealed novel structural configurations that extend beyond previously reported forms, predicting new phases across bulk crystals, nanostructures, and heterojunctions, appearing as novel polytypes. Polytypism refers to the occurrence in which a chemical compound forms crystals in multiple periodically repeated layered configurations (i.e., the polytypes) and is commonly found in II-VI compound semiconductors due to the flexibility in the atomic arrangement of layers made up of cations and anions. [31-36] Although around 200 stacking variants of chemically related ZnS have been experimentally identified, ZnO is known to have only three experimentally observed bulk phases: wurtzite and sphalerite under standard conditions, along with a rocksalt phase under high pressures.

[37-40] However, several newly predicted ZnO polytypes have been reported, [41-44] together with mixed ZnOS crystal structures and polytypes [45-48], as well as various heterostructures. [49-51] Insofar as there is only one crystal structure found in the literature of calcium zinc oxysulfide, denoted as CaZnOS *exp* modification. Consequently, it would be highly advantageous to discover new CaZnOS modifications and polytypes with distinct properties that could also be tuned by altering polytypic formation.

In this study, a multidisciplinary approach has been used to explore the CaZnOS chemical system, combining theoretical and experimental techniques. [52-54] In particular, we employed density functional theory (DFT) from first principles, using five different functionals (LDA−PZ, GGA−PBE, B3LYP, PBE0, and HSE06) to ensure accuracy. The CaZnOS compound was synthesized at high temperature, and its structure was confirmed by X-ray powder diffraction. To discover new CaZnOS configurations, we used novel PCAE and KOVIN structure-prediction algorithms and then evaluated each polytype's stability, electronic, and vibrational properties.

2. Computational and experimental methods

2.1. Structure prediction and Crystallographic analysis

The search for new modifications, compounds, and materials was conducted using crystal structure prediction and energy landscape concepts [55-57], with a special approach for materials under extreme conditions [58, 59]. In particular, the Primitive Cell approach for the Atom Exchange (PCAE) method was used to create various CaZnOS polytypes. The PCAE method is simple, fast, and computationally inexpensive compared to the supercell approach. [46, 60] The method starts by converting the conventional crystallographic cell into its primitive form, the smallest possible unit cell, while preserving atomic symmetry and multiplicity. Transformation matrices for Bravais lattices are sourced from standard codes such as CRYSTAL [61, 62] and KPLOT [63], ensuring consistency with the International Tables for Crystallography [61]. After defining the primitive cell, we perform cation exchange by replacing specific atoms at symmetry-related Wyckoff positions to reach the targeted polytypic structure. Starting with a specific structure, one often finds multiple ion subsets that allow substitution while preserving the space-group symmetry, resulting in a variant of the specific CaZnOS polytype. Finally, we conduct a full *ab initio* structure optimization without symmetry constraints. The recently developed KOVIN (Keep Original Vectors In New structure) algorithm was used to get correct symmetry and undistorted polytypic structures. [62, 63] This method efficiently solves the long-standing challenge of approximating partial occupancy and high symmetry in theoretical calculations of crystal structures. The KOVIN method uses an eight-step transformation and relaxation process to determine the highest symmetry of a given polytype. In this study, the PCAE method was used as the primary tool for generating new polytypes and variants, while the KOVIN algorithm was used as a supplemental tool to analyze and construct undistorted structures (with the original prototype symmetry). For further examples of the successful implementation of the PCAE and KOVIN algorithms, please refer to the existing literature [54, 64, 65]. The periodic simulation cell and atomic positions were allowed to change without enforcing symmetry constraints during local structural optimization for all predicted polytypes and variants. After optimization, the symmetries of the selected structure candidates were established using the SFND [66] and RGS [67] algorithms,

and duplicate structures were identified using the CMPZ [68] algorithm. These three algorithms are incorporated into the KPLOT software [69], which, together with the VESTA [70] program, is used for structural analysis and visualization.

2.2. Structure optimization on the ab initio level

The CRYSTAL code (versions 17 and 23), which employs linear combinations of atomic orbitals, was used for local *ab initio* optimizations. [71, 72] Full structural relaxation was conducted without symmetry constraints to assess the stability of the structures. The local optimizations employed analytical gradients with respect to atom positions [73] and cell parameters [74], as well as a local optimization routine. [73] DFT calculations conducted in the present study employed the Generalized Gradient Approximation (GGA) with the PBE (Perdew, Burke, and Ernzerhof) functional [74], as well as the Local Density Approximation (LDA), with the Slater local exchange approximation [75, 76] and Perdew-Zunger (PZ) correlation functionals. [77]

In addition, three hybrid functionals were used: B3LYP, HSE06, and PBE0. B3LYP is the Becke's three-parameter functional combined with the correlation functional of Lee, Yang, and Parr. [78] The hybrid HSE06 (Heyd-Scuseria-Ernzerhof) exchange-correlation functional uses an error-function-screened Coulomb potential to calculate the exchange portion of the energy to improve computational efficiency, [79] while the PBE0 functional mixes the Perdew–Burke-Ernzerhof (PBE) exchange energy and Hartree–Fock exchange energy in a 3:1 ratio, along with the full PBE correlation energy. [80, 81] This is very important, as repeating local optimizations across various *ab initio* methods helps assess the quantitative accuracy and reliability of the computed data. [82-84]

2.3. Basis sets and phonon calculations

All-electron basis sets (AEBS) based on Gaussian-type orbitals (GTO) were utilized. For Zn^{2+}, a [6s5p2d] basis set was used, as in refs. [85-87], while for the Ca^{2+}, a [*5s4p1d*] basis set was used as in refs. [88, 89] For O^{2-}, a [*4s3p*] basis set was used as in refs. [85, 90, 91]. For S^{2-}, an *[5s4p1d]* all-electron basis set was used as in refs. [92, 93], while combinations of these basis sets were used as described in ref. [46]. A *k*-point sampling net of size 8 × 8 × 8 was used. Vibrational properties and thermodynamic stability were determined using a supercell method implemented in the CRYSTAL code. [94, 95] To attain optimal computational efficiency and maintain the calculations manageable, supercells of the dimensions 2 × 2 × 2 were employed for the different orientations. The SCF convergence criterion for total energy was set to 10^{-9}. A supercell large enough was chosen, and the SCF convergence criterion was precise enough to ensure reliable interpolation along all directions. The phonon spectrum was computed on 64 *k*-points along 7 reciprocal space directions using a shrinking factor of 6. Labels and coordinates of the special points with the highest symmetry for each Bravais lattice correspond to the hexagonal (*hcp*) lattice.

2.4. Synthesis

For the synthesis of CaZnOS, the starting precursors were $CaCO_3$ analytical grade (p.a.) and previously prepared ZnS (according to the literature [52]). The desired phase was formed by a solid-state reaction in an inert argon atmosphere at 1000 °C. The general reaction is:

$$CaCO_3 + ZnS \longrightarrow CaZnOS + CO_2 \quad (1)$$

The process involved mixing stoichiometric amounts of finely ground precursors, pressing them into pellets, and annealing at 1000 °C for 2 hours to obtain single-phase CaZnOS, while carefully controlling temperature to avoid sulfur loss or the formation of side phases such as CaS and ZnO.

2.5. Materials Characterization

The synthesized CaZnOS samples were characterized by X-ray powder diffraction (XRPD) using a Rigaku Ultima IV diffractometer with Cu Kα radiation and a Ni filter. To derive the relevant structural parameters, experimental data were collected at a scan rate of 2° 2θ per minute over a range of 2θ (10–90º), with an angular resolution of 0.02 º2θ. Structural analysis was accomplished using the ICSD database, Rietveld refinement, and the program FullProf. [96, 97]

3. RESULTS

3.1. Crystal structures and structural features of CaZnOS

In this section, we present calculated and synthesized crystal structures of CaZnOS. Specifically, the calculated crystal structure using *ab initio* methods from experimentally observed CaZnOS structure type is shown in section 3.1.1, followed by newly predicted models of the crystal structures in the 2H polytype (section 3.1.2), 4H polytype (section 3.1.3), 8H polytype (section 3.1.4), and 12R polytype (section 3.1.5). Finally, the experimental CaZnOS crystal structure and XRPD results are presented in section 3.1.6.

3.1.1. Calculated crystal structure from experimentally observed CaZnOS modification

Due to its distinctive structural and functional characteristics, calcium zinc oxysulfide (CaZnOS) emerges as a material of particular scientific interest. It belongs to the family of layered oxysulfides (space group $P6_3mc$), combining oxide and sulfide characteristics in a non-centrosymmetric hexagonal lattice. [98, 99] The crystal structure consists of alternating layers of ZnS and CaO polyhedra, in which oxygen and sulfur occupy distinct anion sites. The atoms are arranged in layers packed along the [001] direction. Such layers are constructed so that Zn is tetrahedrally coordinated by three S atoms, forming a section of the ZnS layer, and by one O atom from the adjacent CaO layer. On the other hand, the coordination number of Ca is 6 (3 oxygen and 3 sulfur atoms), forming a distorted octahedron in the next layer (Fig. 1). [98, 99]

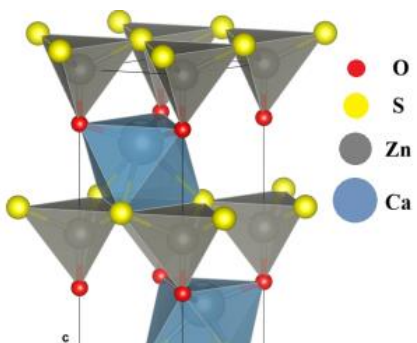

Fig. 1. Crystal structure of the experimentally observed CaZnOS modification (so-called CaZnOS-*exp* type). Zinc atoms are presented in gray color, calcium in blue, oxygen in red, and sulfur in yellow.

Experimentally observed CaZnOS-*exp* type structure (Fig. 1) was computed using DFT-LDA and GGA-PBE as well as hybrid HSE06, B3LYP, and PBE0 functionals. Calculated structural data (space group and unit cell parameters) and band gap values are shown in the supporting information (Table S1). The CaZnOS-*exp* type was fully optimized and after full relaxation, the structure remained in the experimentally observed hexagonal $P6_3mc$ (no. 186) space group, with unit cell parameters a = 3.75 Å, c = 11.49 Å using HSE06; a = 3.68 Å, c = 11.15 Å using LDA; a = 3.78 Å, c = 11.64 Å using B3LYP; a = 3.76 Å, c = 11.53 Å using GGA-PBE, and a = 3.75 Å, c = 11.49 Å using PBE0 methods. Each result concur with present experimental data, however the best agreement to the XRD data is found with hybrid HSE06 functional (XRD unit cell parameters are a = 3.7570(2) Å; c = 11.3968(9) Å, and previously reported XRD values of a = 3.75726(3) Å, c = 11.4013(1) Å [98], and a = 3.7547(1) Å, c = 11.4014(5) Å [99].

We note that the experimentally observed CaZnOS modification can be further engineered to modify its structural and electronic properties by replacing possible cation and anion positions within the crystallographic unit cell. Thus, experimentally observed CaZnOS-*exp* structure has the atom arranged in the next order (1) Zn (2) Ca (3) S (4) O and marked as V1 variant (see supporting information Table S2 and Fig. S1). The V2 variant has the order of (1) Zn (2) Ca (3) O (4) S, the V3 variant has the order of (1) Ca (2) Zn (3) O (4) S, and V4 variant has the order of (1) Ca (2) Zn (3) S (4) O (Table S2 and Fig. S1). After performing full structural relaxation on the DFT level, all structural variants remain the CaZnOS-*exp* structure type, as observed from experiments, confirmed by KPLOT and the CMPZ algorithm. In addition, we have computed two more variants, V5 and V6, in the primitive unit cell, replacing atoms that do not belong to the asymmetric unit cell (Table S2 and Fig. S1). An atom belonging to the asymmetric unit is part of the smallest unique crystal fragment that, when symmetry operations are applied, generates the entire repeating unit cell, containing atoms that define the crystal's structure without redundancy (Figs. S1-S5). However, since we used the PCAE method and replaced the atoms outside the asymmetric unit cell, we reduced the symmetry to the hexagonal $P3m1$ (no. 156) space group (Table 2). After creating energy vs. volume, $E(V)$, curves for all structural variations of the CaZnOS-*exp* type marked V1-V6, we note that the V1 variant, which is experimentally observed, is the lowest energy minimum (Fig. 2).

Table 2. Calculated structural data (space group and unit cell parameters) and band gap values for the considered variants of the *exp* type in CaZnOS. The calculations were performed using the hybrid HSE06 functional.

CaZnOS-*exp* type	V1	V2	V3	V4	V5	V6
Space group, unit cell parameters (Å)	*Sg 186* *P6$_3$mc* *a* = 3.75; *c* = 11.49	*Sg 186* *P6$_3$mc* *a* = 3.59; *c* = 12.35	*Sg 186* *P6$_3$mc* *a* = 3.75; *c* = 12.10	*Sg 186* *P6$_3$mc* *a* = 3.64; *c* = 12.13	*Sg 156* *P3m*1 *a* = *3.71;* *c* = *11.79*	*Sg 156* *P3m*1 *a* = 3.67; *c* = 11.95
Band gap (eV)	4.50	0.54	3.89	2.53	3.94	3.51

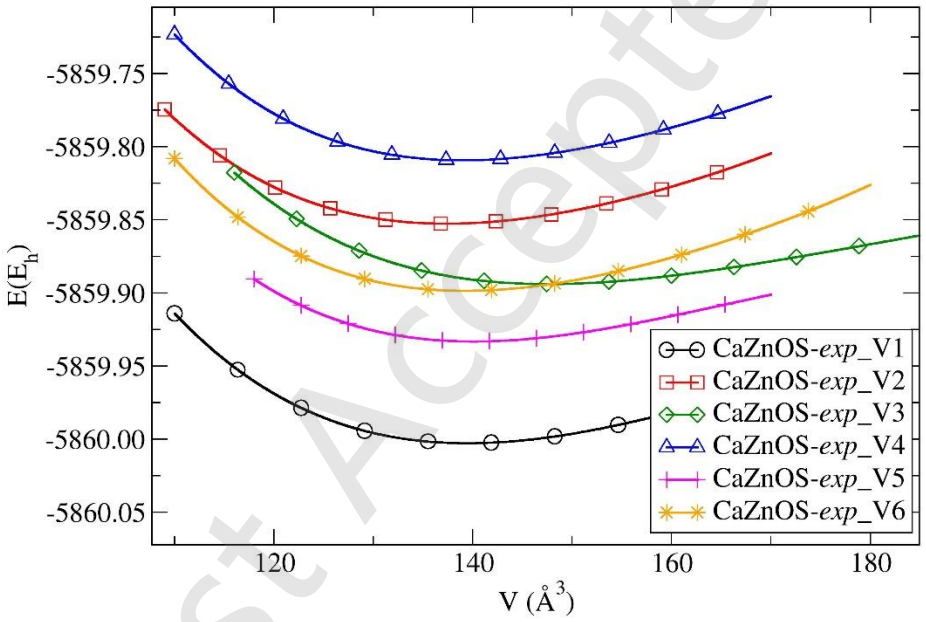

Fig. 2. Energy vs. volume, *E(V)*, curves for the structural variations of the CaZnOS-*exp* type marked V1-V6. The calculations were performed using the hybrid HSE06 functional.

However, the structural data, unit cell parameters, and atomic positions differ, as does the computed band gap (Full structural data are provided in SI Table S3). Calculations using the hybrid HSE06 functional yielded a band gap of 4.50 eV for the V1 variant, whereas for the V2 variant it was reduced to 0.54 eV. Other variants allow tuning the band gap between these values, and the V3 variant shows a band gap of 3.89 eV and concurs with the measured band gap of 3.7 eV [98] as well as with previous GGA-PBE calculations of 3.90 eV. [100]

3.1.2. 2H polytype

The CaZnOS-*exp* structure type observed in experiment appears to be polytypic, with alternating Ca and Zn layers. The smallest possible polytype in the literature from related ZnO and ZnS systems is the 2H polytype crystallizing in the hexagonal $P6_3mc$ (no. 186) space group with the wurtzite structure. [38, 85, 101-103] In this study, we have used the PCAE method and the 2H polytype from a related ZnO/S compound, [46, 47] replacing one Zn by one Ca atom, and reducing symmetry to the hexagonal $P3m1$ (no. 156) (Fig. 3), to create a 2H polytype of CaZnOS. The predicted crystal structure and XRD data of the 2H polytype are clearly different from the CaZnOS-*exp* type (Fig. 3). Thus, the family of the CaZnOS-*exp* structure is clearly different from the ZnO/S based family of structures.

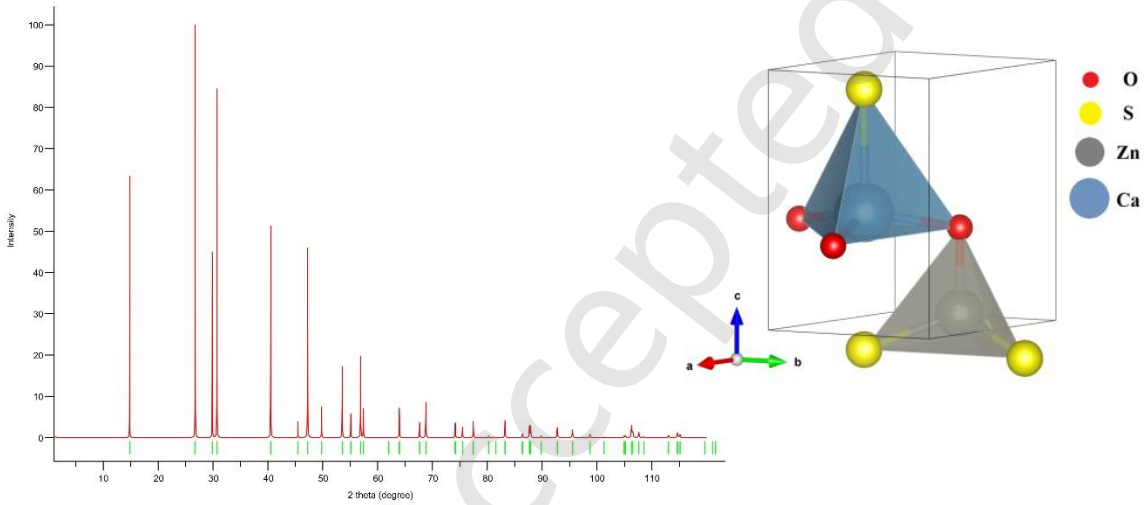

a) b)

Fig. 3. Predicted 2H polytype: a) powder diffraction pattern; b) crystal structure visualization. Zinc atoms are presented in gray color, calcium in blue, oxygen in red, and sulfur in yellow.

To further study all possible modifications to the predicted 2H polytype in CaZnOS, we have generated only four possible variants of the 2H CaZnOS marked from V1-V4 (see supporting information Fig. S2, and Tables S4 and S5 for full structural details). Again, after accomplishing full structural relaxation on an *ab initio* level, all four structural variants remain the 2H polytype in the hexagonal $P3m1$ (no. 156) symmetry (Table 3). After creating the $E(V)$ curves for all structural variations of the 2H polytype marked V1-V4, we note that the V1 variant is the lowest energy minimum (Fig. S6 in the SI). Moreover, the V3 variant converges to the V1 minimum, with the exact total energies, while V4 converged to the high energy minimum V2, making the V1 variant the only possibility for the 2H polytype. Unlike the experimentally observed CaZnOS-*exp* type, the 2H polytype shows only one variant as the most relevant 2H structure, with a possible band gap of 4.53 eV computed with the hybrid HSE06 functional. The V2 (and V4) modifications show a band gap of 1.79 eV, but are unlikely to be experimentally realized in CaZnOS with a 2H polytypic structure. Moreover, the band gap of the 2H V1 variant has been computed from 3.21 eV using LDA to 5.19 eV using the hybrid PBE0 functional (Table S1 in the SI).

Table 3. Computed structural data (space group, unit cell parameters, atomic positions) and band gap value for the only relevant modification of 2H polytype in CaZnOS. The calculations were performed using the hybrid HSE06 functional.

2H	V1 (=V3)
Space group, unit cell parameters (Å), atomic positions	*Sg 156* *P*3*m*1 *a* = 3.85; *c* = 5.98 Zn 1/3 2/3 0.0409 Ca 2/3 1/3 0.4406 O 1/3 2/3 0.3697 S 2/3 1/3 0.9129
Band gap (eV)	4.53

On the other hand, we would like to note that a recent study by Zhang et al. reports that the wurtzite (2H) polytype serves as a host for CaZnOS (an artificial variant of ZnS), which crystallizes in a non-centrosymmetric hexagonal lattice (space group $P6_3mc$).[28] We have modeled such a 2H polytype in the ideal hexagonal space group P63mc (no. 186) using the KOVIN algorithm. The resulting structural details are shown in the supporting information (Table S6), in agreement with previous reports [28]. We note that the higher band gap values (4.10 eV and 3.07 eV) obtained for hexagonal symmetry are closer to the measured value of 3.7 eV [100] and to previous PBE calculations of 3.90 eV for the CaZnOS-*exp* type of structure. [100] Furthermore, the high doping capacity and wide bandgap of this structure provide ample room for engineering defects and luminescent centers. [27, 28, 104]

3.1.3. 4H polytype

The 4H polytype structure is well known in related chemical systems, including zinc sulfide, zinc oxide, and ZnOS. [37, 42, 43, 47, 52, 105-107] The 4H crystal structure in CaZnOS was created from the 4H ZnS structure by substituting one Zn atom with one Ca atom in the crystallographic unit cell, resulting in a structure that consists of alternating layers of Zn and Ca coordinated polyhedra (ZnS and CaO tetrahedra). These layers are constructed in such a way that Zn and Ca atoms are tetrahedrally coordinated by O and S atoms, in contrast to the CaZnOS-*exp* structure, where Zn atoms are tetrahedrally coordinated, and Ca atoms are octahedrally coordinated by O and S atoms, respectively. Moreover, the predicted XRD of the 4H and CaZnOS-*exp* type are clearly different (Fig. 4). [42, 98]

a) b)

Fig. 4. Predicted 4H polytype: a) powder diffraction pattern; b) crystal structure visualization. Zinc atoms are presented in gray color, calcium in blue, oxygen in red, and sulfur in yellow.

Similar to the experimentally observed CaZnOS-*exp* type, the 4H polytype can be modified and engineered to alter its structural and electronic properties by replacing possible cation and anion positions within the crystallographic unit cell. Initially, we have created four modifications of 4H polytype: (1) Zn (2) Ca (3) S (4) O, and marked as V1 variant (see supporting information Table S5 and Table 4). The V2 variant has the order of (1) Zn (2) Ca (3) O (4) S, the V3 variant has the order of (1) Ca (2) Zn (3) O (4) S, and V4 variant has the order of (1) Ca (2) Zn (3) S (4) O (Table S7). After performing full structural relaxation at the *ab initio* level, all structural variants remain the 4H polytype; the V2 converges to the V1 variant, and the V4 converges to the V3 variant, leaving only two distinct variants, V1 and V3. In addition, we computed several variants from the primitive unit cell by replacing atoms not belonging to the asymmetric unit cell, and subsequently performed full structural relaxation in P1 using the hybrid HSE06 functional (Tables 4, S7, and S8, and Fig. S3 in the SI). After computing *E(V)* curves for all structural variations of the 4H polytype, we note that the V1 variant is the lowest energy minimum. In contrast, V5 and V6 variants from the PCAE models were energetically favorable, below the V2 variant (Fig. 5). Again, due to the usage of the PCAE method and initial structures from ZnO/S compound, the symmetry of the new V5 and V6 variants was reduced to the hexagonal *P*3*m*1 (no. 156) space group (Table 4).

Table 4. Computed structural data (space group and unit cell parameters) and band gap value for the considered variants of 4H polytype in CaZnOS. The calculations were performed using the hybrid HSE06 functional.

4H	V1 (=V3)	V2 (=V4)	V5	V6
Space group, unit cell parameters	*Sg 186* *P6₃mc*	*Sg 186* *P6₃mc*	*Sg 156* *P3m*1	Sg 156 *P3m1*

(Å)	a = 3.84; c = 11.96	a = 3.73; c = 12.97	a = 3.77; c = 12.58	a = 3.79; c = 12.75
Band gap (eV)	4.55	1.78	2.92	1.58

We would like to note again that structural data, unit cell parameters, and atomic positions differ, as does the computed band gap (Tables 4 and S8). The calculations using the hybrid HSE06 functional resulted in a band gap of 4.55 eV for the V1 variant, 1.58 eV for the V6 variant, and 2.92 eV for the V5 variant. Furthermore, the V1 variant exhibits a band gap ranging from 3.24 eV, computed using the GGA-PBE functional, to 5.21 eV, obtained using the hybrid PBE0 functional (Table S1 in the SI). The 4H polytype of CaZnOS is unreported and could be an excellent intermediate between the experimentally observed CaZnOS-*exp* type [100] and the wurtzite (2H) polytype observed in recent experiments [28].

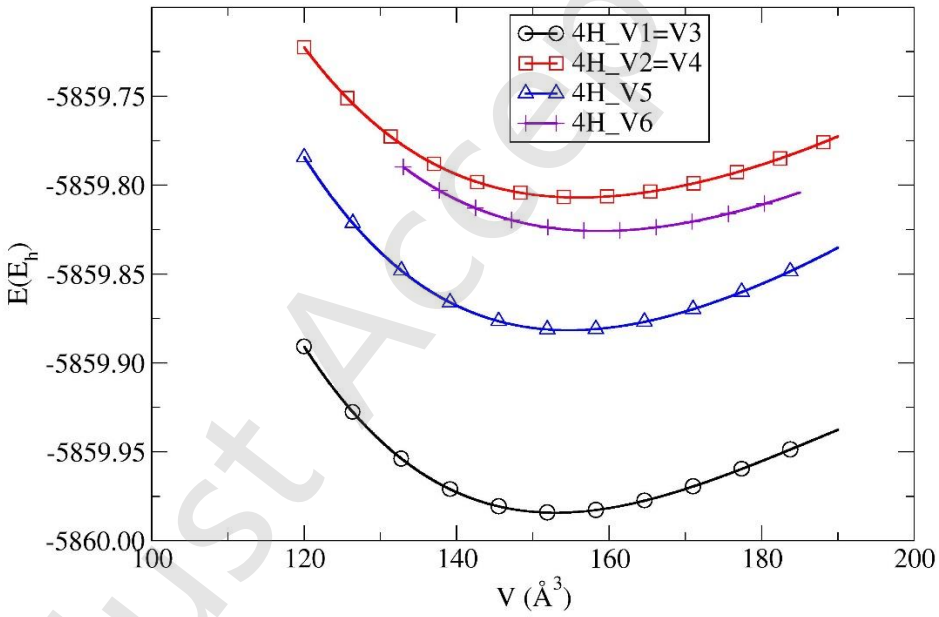

Fig. 5. Computed *E(V)* curves for the structural variations of the 4H polytype in CaZnOS marked V1-V6. The calculations were performed using the hybrid HSE06 functional.

3.1.4. 8H polytype

The 8H polytypic structure refers to a specific crystal structure of zinc sulfide, a form of polytypism where the atoms stack in an eight-layer (8H) hexagonal pattern, distinct from the more common 2H (wurtzite) or 3C (sphalerite) structures or from previously computed 4H polytype, appearing in various inorganic compounds, such as SiC, ZnO, ZnS, ZnOS, etc [37, 42, 43, 47, 52, 105-110] The 8H polytype of CaZnOS was created from 8H ZnS, as well as from the ZnO/S using PCAE method, by replacing zinc atoms with calcium atoms. This procedure generated several variants of the 8H polytype, marked V1-V6, resulting in polytypic structures consisting of alternating layers of mixed ZnS/O and CaO/S tetrahedra (see supporting information, Fig. S4, and Tables S9 and S10 for full structural data). The 8H polytype is different from previously computed CaZnOS modifications, as shown in the powder diffraction pattern and crystal structure visualization (Fig. 6).

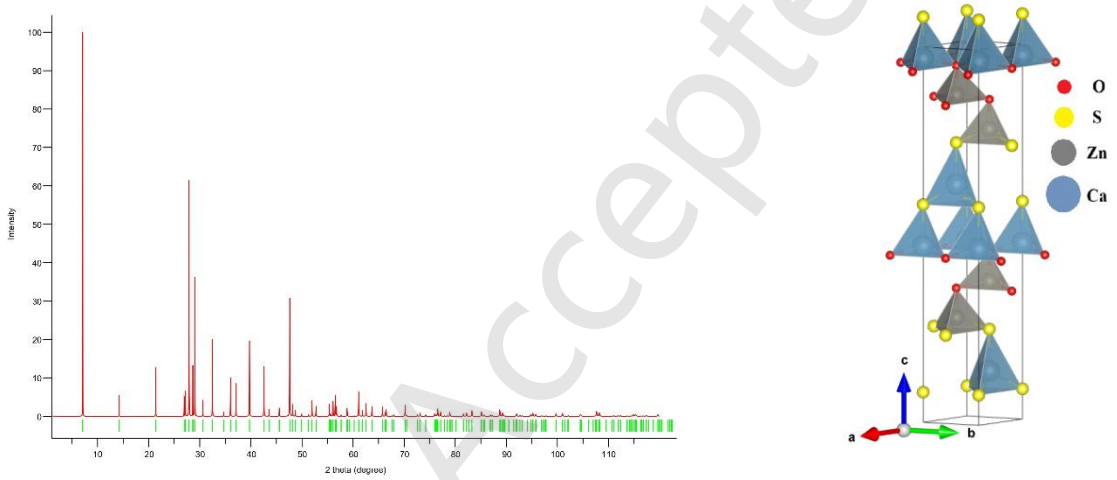

a) b)

Fig. 6. Predicted 8H (V2) polytype: a) powder diffraction pattern; b) crystal structure visualization. Zinc atoms are presented in gray color, calcium in blue, oxygen in red, and sulfur in yellow.

After *ab initio* structural relaxation and calculations of the *E(V)* curves for all structural variations of the 8H polytype in CaZnOS, we note that the V2 variant is the lowest energy minimum, closely followed by the V4 variant on the energy landscape, while V1 and V3 represent the same energy minimum. The structures originated from the ZnO/S chemical system created from PCAE have much higher energies, and we have manged to include the V5 variant in the *E(V)* curves, while V6 variant was energetically even higher and, thus, was not included (Fig. 7). Although the symmetry of the structures generated from the primitive unit cell remained hexagonal $P6_3mc$ (no. 186), all 8H variants exhibit slight distortions, resulting in deformed tetrahedra in the layers (Fig. 6b). This could be indication of the instability of the 8H polytype in the CaZnOS system.

When we further analyze the structural data for the 8H CaZnOS polytype, the unit cell parameters and atomic positions differ across all computed variants, except for V1 and V3. Although the V2 and V4 variants are very close on the energy landscape (Fig. 7), we note

differences in structural data and the calculated band gap. In principle, by arranging different positions of the Ca and Zn atoms in the V2 and V4, one could reduce the band gap from 3.02 eV to 2.61 eV at the HSE level of calculations. If we adopt a more random ordering of atoms in the primitive cell, as in the V5 variant, it could be reduced to 1.67 eV (Table 5); however, this is unlikely given the computed high total energy and the structure's metastability. On the other hand, if we keep the V2 variant and change the DFT method, the band gap can be further varied from 1.77 eV using LDA to 3.69 eV using the hybrid PBE0 functional (Table S1 in the SI).

Table 5. Computed structural data (space group and unit cell parameters) and band gap value for the considered variants of 8H polytype in CaZnOS. The calculations were performed using the hybrid HSE06 functional.

8H	V1=V3	V2	V4	V5
Space group, unit cell parameters (Å)	*Sg 186* $P6_3mc$ $a = 3.75$; $c = 25.16$	*Sg 186* $P6_3mc$ $a = 3.82$; $c = 24.91$	*Sg 186* $P6_3mc$ $a = 3.80$; $c = 25.10$	*Sg 186* $P6_3mc$ $a = 3.75$; $c = 25.92$
Band gap (eV)	2.26	3.02	2.61	1.67

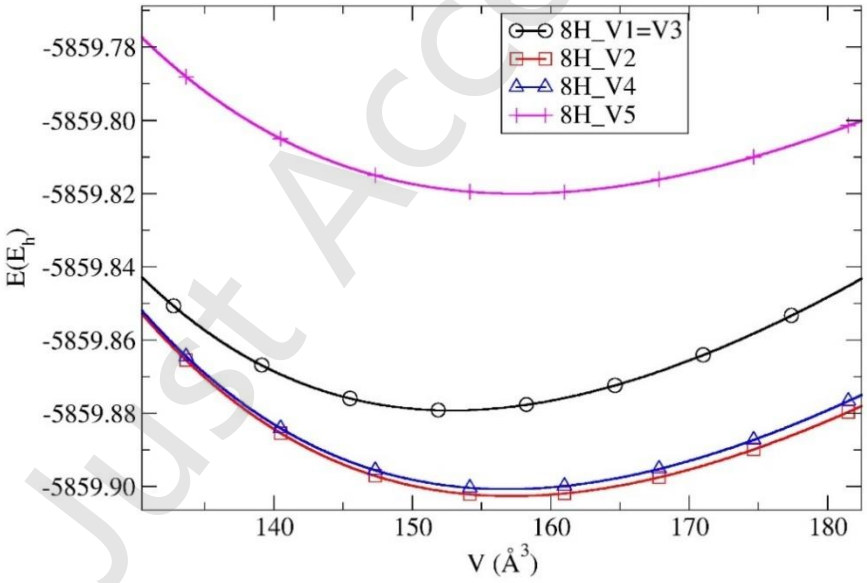

Fig. 7. Computed *E(V)* curves for the structural variations of the 8H polytype in CaZnOS marked V1-V5. The calculations were performed using the hybrid HSE06 functional.

3.1.5. 12R polytype

The 12R polytype is a layered structure consisting of 12 atomic layers, with the pattern repeating after every 12 layers. This polytype is frequently observed in various materials, such as CdI_2, ZnO, ZnS, ZnOS, and perovskites [37, 42, 43, 47, 52, 105-107, 111-113]. The 12R polytype

is distinguished from the previously calculated ones by its rhombohedral symmetry (*R*3*m*) and unique stacking patterns, which influence its electronic, magnetic, and physical properties. These arrangements result from different atomic stacking sequences, where 'R' denotes rhombohedral and '12' denotes 12 layers, in contrast to the hexagonal (H) polytype.

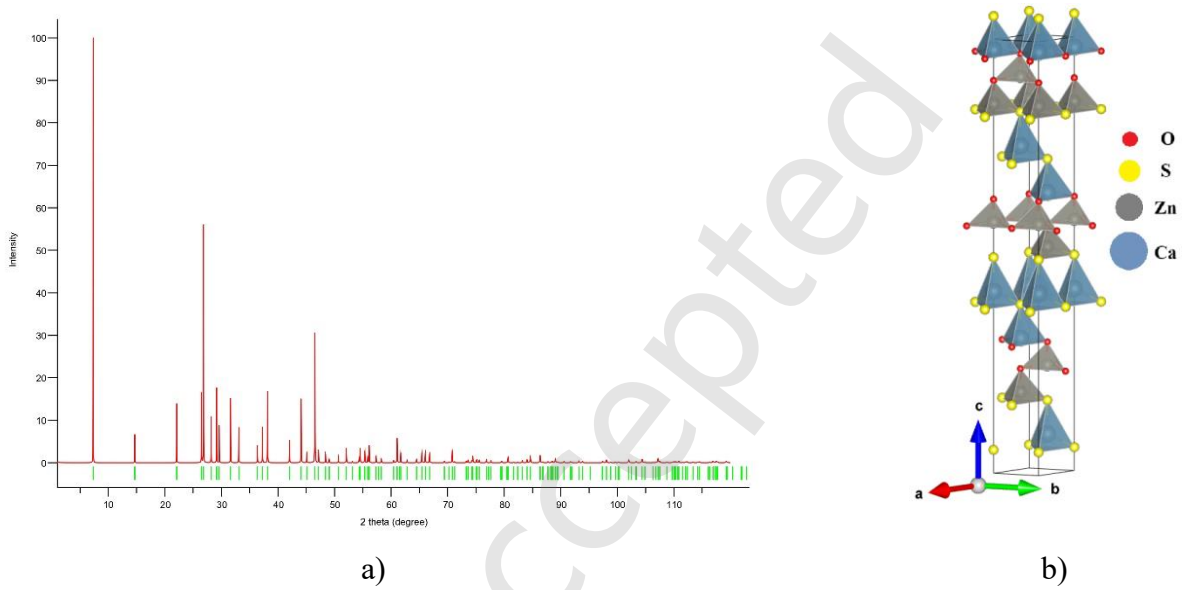

a) b)

Fig. 8. Predicted 12R (V2) polytype: a) powder diffraction pattern; b) crystal structure visualization. Zinc atoms are presented in gray color, calcium in blue, oxygen in red, and sulfur in yellow.

The 12R polytype of CaZnOS was generated from the 12R model in the ZnS and ZnO/S systems using the PCAE method, by replacing zinc atoms with calcium atoms. Again, we can obtain several variants of the 12R polytype, marked V1-V6 (Table S11). However, after *ab initio* structural optimization, all computed variants were significantly distorted from the ideal 12R polytype. As a result, all calculated variants of 12R polytype show layers of various shapes and sizes, with strongly distorted Ca and Zn polyhedra (Fig. 8 and S5), in contrast to the initial 12R polytypic structure, which consists of alternating layers of ZnS tetrahedra (see supporting information Table S11 and S12 for full structural data). Moreover, the 12R polytype is different from previously computed CaZnOS polytypes, as shown in the powder diffraction pattern and crystal structure visualization (Fig. 8). On the other hand, all computed variants V1-V6 are the same structure type, confirmed by KPLOT and CMPZ algorithm, representing a completely new polytype not previously observed in any known chemical system.

Table 6. Computed structural data (space group and unit cell parameters) and band gap value for the considered variants of the 12R polytype in CaZnOS. The calculations were performed using the hybrid HSE06 functional.

12R	V1	V2	V3	V4	V5

Space group, unit cell parameters (Å)	*Sg 160 R3m* a = 3.76; c =37.50	*Sg 160 R3m* a = 3.90; c =36.16	*Sg 160 R3m* a = 3.75; c =37.74	*Sg 160 R3m* a = 3.80; c =37.66	*Sg 160 R3m* a = 3.80; c =37.30
Band gap (eV)	2.42	3.20	3.39	2.60	3.16

Interestingly, when further analyzing structural data, unit cell parameters and atomic positions are different for all computed variants of the 12R CaZnOS polytype except for V1 and V3 variants, although different in computed total energies (Fig. 9). Similarly, V4 and V5 variants have the same unit cell parameters, but they are different minima on the energy landscape (Fig. 9), as well as different size of the calculated band gap (Table 6). The lowest energy minimum corresponds to the V2 variant with a band gap of 2.42 eV, while other variations of the same 12R polytype could result in a band gap from 1.78 to 3.39 eV (Table 6 and S12), while by using the V2 variant, and changing the functional, the band gap could result from 1.96 eV using LDA to 3.89 eV using hybrid PBE0 functional (Table S1 in the SI).

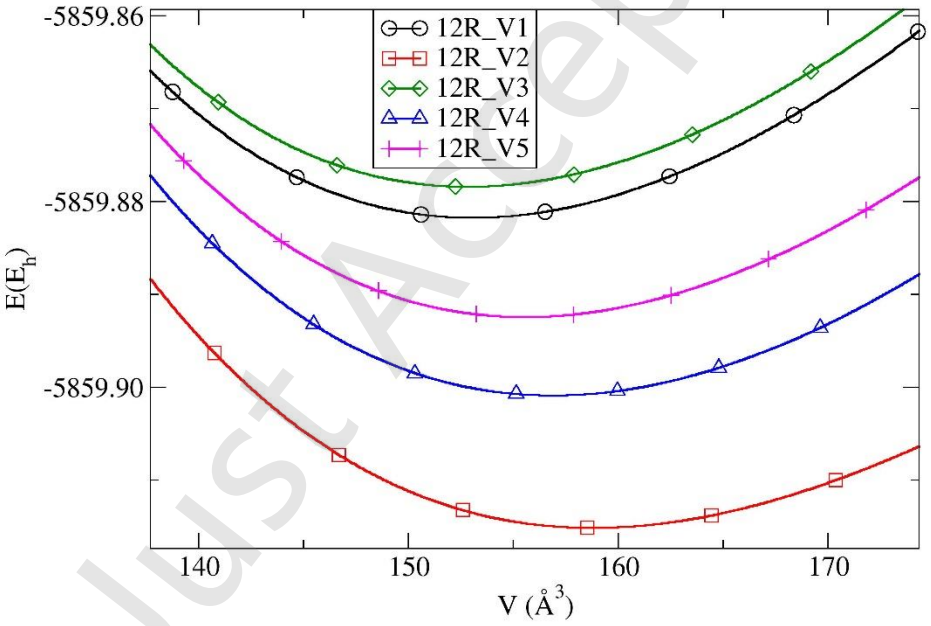

Fig. 9. Computed *E(V)* curves for the structural variations of the 12R polytype in CaZnOS marked V1-V5. The calculations were performed using the hybrid HSE06 functional.

3.1.6. Experimental CaZnOS crystal structure and XRPD results

Rietveld refinement has been performed starting from the CaZnOS structure model reported in 10.1023/B:DOCH.0000003458.35866.40, (ICSD #250092). [99] The crystal structure

of CaZnOS, designated as CaZnOS-*exp* type in this study, exhibits non-centrosymmetric hexagonal symmetry with the space group of $P6_3mc$, and refined atomic positions are given in Table 7. Zinc and oxygen atoms occupy the 2(a) positions, while calcium and sulfur are in the 2(b) positions. Unit cell parameters are a = 3.7570(2); c = 11.3968(9). This is in excellent agreement with previous reported values of a = 3.7547(1) Å, c = 11.4014(5) Å, [99] and a = 3.75726(3) Å, c = 11.4013(1) Å. [98] Refined atomic positions for CaZnOS *exp* type (Table 7) are also in very good agreement with literature data. [99, 114]

Table 7. Refined atomic positions of the crystal structure of CaZnOS-*exp* modification exhibiting non-centrosymmetric hexagonal symmetry with the space group of $P6_3mc$.

Atom	*x*	*y*	*z*
Zn	0	0	0.8494(3)
Ca	1/3	2/3	0.1180(3)
S	1/3	2/3	0.4315(3)
O	0	0	0.1754(5)

A Rietveld diagram of CaZnOS powders obtained after heating at 1000 °C for 2 hours is shown in Fig. 10. Quantitative phase analysis revealed that the main CaZnOS phase is abundant at 85.9(4) %, and the second phase accounts for 14.1(1) %. In the second phase, CaO crystallizes in the *Fm-3m* space group, with a = 4.8096(7). The ~14% CaO secondary phase may partially influence the interpretation, but the main conclusions about the predicted structures and their stability are based on DFT calculations of the pure CaZnOS system. The synthetic conditions were optimized to obtain the experimentally known structure type, while the formation of new CaZnOS polytypes under modified synthesis conditions (e.g., higher temperature and/or pressure) opens new possibilities for future research.

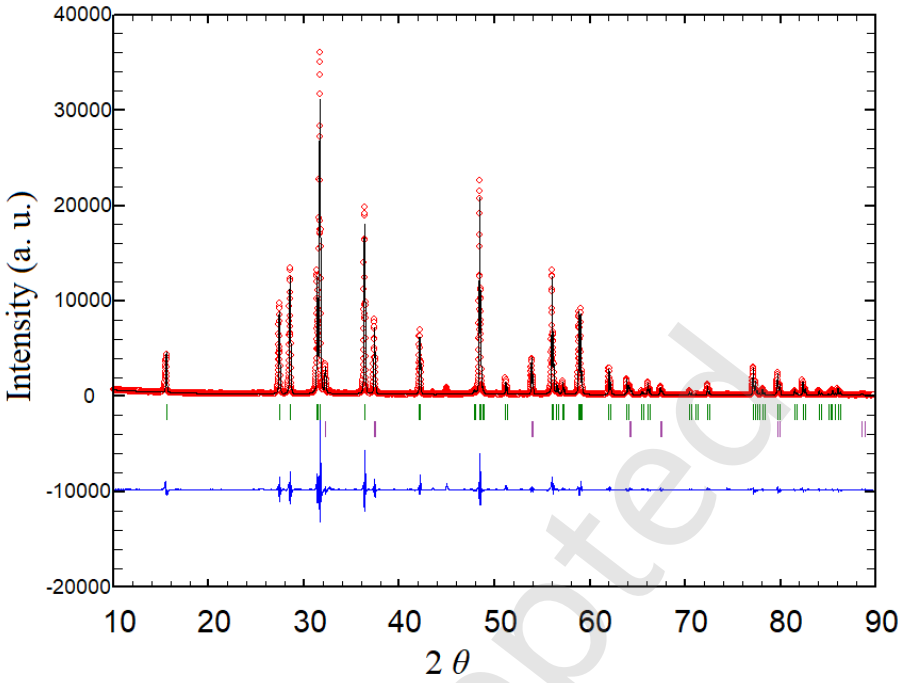

Fig. 10. Rietveld diagram of CaZnOS powders obtained after heating at 1000 °C for 2 hours. The blue line denotes the difference between the experimental (red diamonds) and theoretical (black line) profile, while the Bragg positions are indicated by vertical green and violet slashes. The first row with the green bars corresponds to the diffraction lines of the CaZnOS-*exp* type phase, and the second row with the violet bars corresponds to the CaO phase, respectively.

3.2. Stability of calculated and predicted CaZnOS structures

The stability of calculated polytypic crystal structures is assessed by their computed total energies at the *ab initio* level, with the lowest energy indicating the most stable structure. Key evaluation methods include density functional theory (DFT) for energy minima, analysis of the energy band structure, dynamical stability (phonons), and electronic properties. On the energy landscape of CaZnOS, identifying global minima (ground states) versus shallow local minima (metastable states) is crucial. In the following, we have computed the *E(V)* curves for the most relevant (lowest energy) predicted structures of the CaZnOS using the hybrid HSE06 method (Fig. 11). We note that the CaZnOS *exp* type corresponds to the lowest energy minimum and thus the kinetically most stable structure, in agreement with experimental data. The predicted 2H and 4H polytypes are close in energy on the energy landscape and potentially stable in the low-density region (Fig. 11). On the other hand, 8H and 12R are highly metastable and are expected to be very difficult to synthesize experimentally in the CaZnOS system. The *E(V)* curves were additionally computed using four *ab initio* methods: LDA-PZ, GGA-PBE, hybrid B3LYP, and PBE0 for the lowest-energy predicted structures of CaZnOS. The energy ranking and stability of the polytypes

were confirmed regardless of the computational approach, and other variants are even higher in energy (see supporting information Figs. S7-S10)

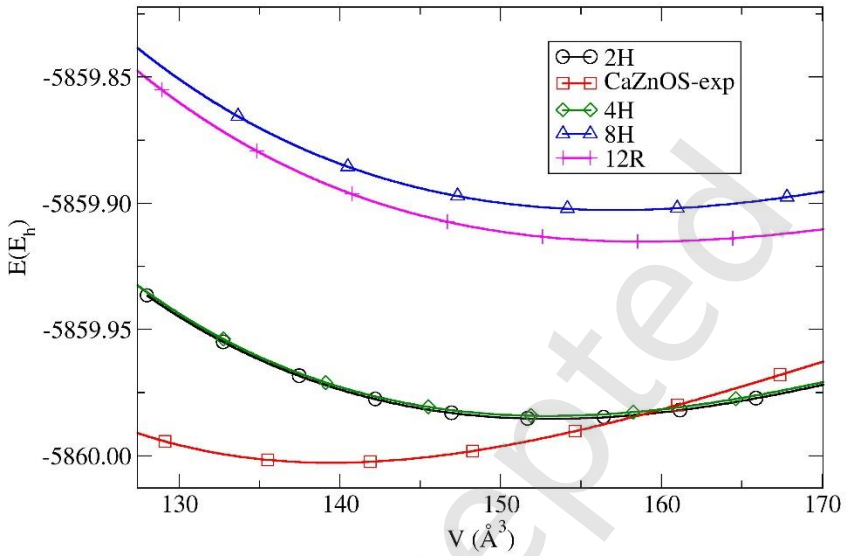

Fig. 11. Computed *E(V)* curves for the most relevant predicted polytypic structures in CaZnOS. The calculations were performed using the hybrid HSE06 functional.

In addition, the formation energies (E_f) of all predicted polytypes and variants of CaZnOS were calculated. Summary of computed formation energies (eV/atom) using the hybrid HSE06 functional is shown in Table 8. We note that all computed structures show negative E_f, indicating stability in agreement with computed *E(V)* curves. Furthermore, the phase diagram of CaZnOS was calculated using Open Quantum Materials Database (OQMD) [115, 116] and presented in the supporting information (Figs. S11 and S12). The E_f are computed using DFT calculations with the VASP code and the GGA-PBE functional, employing the projector-augmented-wave (PAW) method. All computed formation energies of the structures found on the phase diagram of CaZnOS are negative, in agreement with present LCAO hybrid HSE06 calculations.

Table 8. Computed formation energies E_f (eV/atom) and total energies E_{tot} (Ha/f.u.) for all calculated structures, polytypes, and variants of CaZnOS. The calculations were performed using the hybrid HSE06 functional.

Structure/ Polytype	**Energy**	**Variant**					
		V1	V2	V3	V4	V5	V6
2H	E_f	-3.67	-3.07	-3.67	-3.07	n.a.	n.a.
	E_{tot}	-5859.9852	-5859.8086	-5859.9852	-5859.8086	n.a.	n.a.
CaZnOS-*exp*	E_f	-3.72	-3.22	-3.36	-3.07	-3.49	-3.37

	E_{tot}	-5860.0016	-5859.8521	-5859.8931	-5859.8096	-5860.9325	-5859.8985
4H	E_f	-3.67	-3.06	-3.67	-3.06	-3.32	-3.12
	E_{tot}	-5859.9849	-5859.8070	-5859.9849	-5859.8070	-5859.8815	-5859.8251
8H	E_f	-3.31	-3.39	-3.31	-3.38	-3.11	-3.06
	E_{tot}	-5859.8788	-5859.9030	-5859.8784	-5859.9005	5859.8202	-5859.8066
12R	E_f	-3.32	-3.43	-3.31	-3.38	-3.35	-3.06
	E_{tot}	-5859.8815	-5859.9147	-5859.8781	-5859.9004	-5859.8924	-5859.8073

Moreover, we have investigated thermodynamic stability using phonon calculations. Phonon band structures reveal a material's dynamical stability (the absence of imaginary phonon frequencies) and are linked to its overall thermodynamic stability, influencing mechanical, thermal, and electronic properties. Stable phonon bands (positive frequencies) indicate a real crystal structure, whereas imaginary frequencies suggest instability, often leading to phase transitions or decomposition, as demonstrated in previous studies. [84, 100, 117, 118]

a)

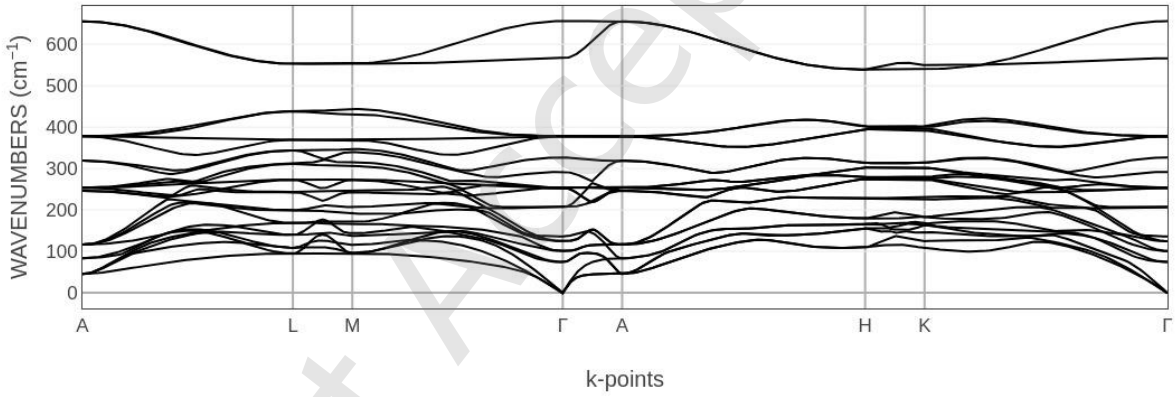

b)

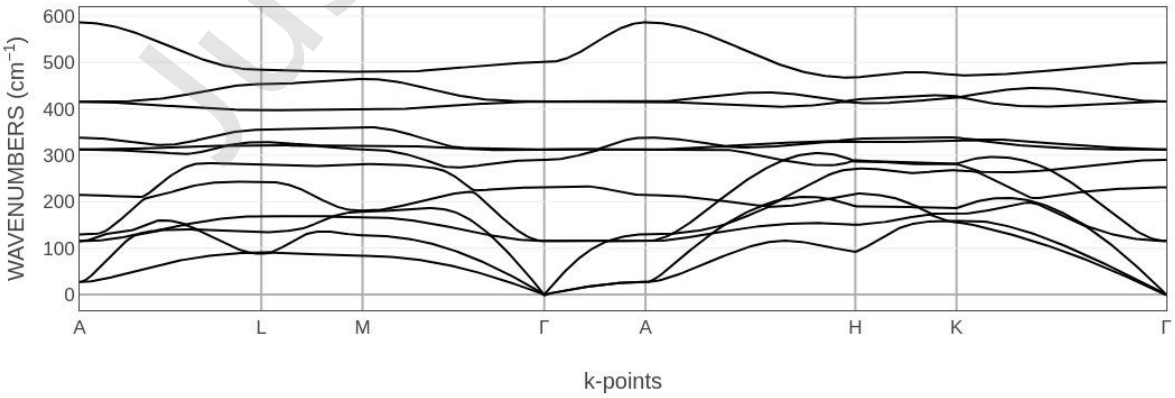

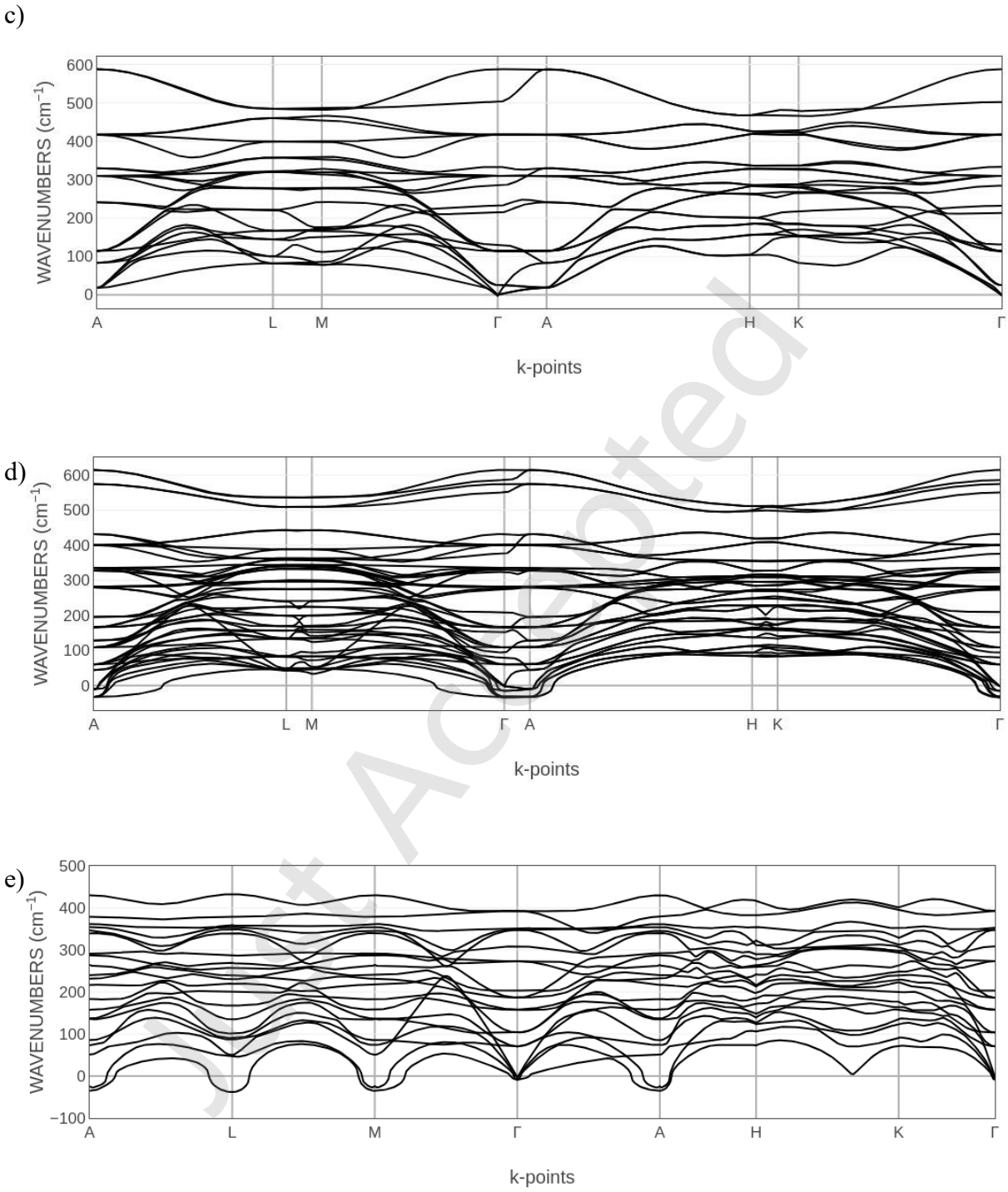

Fig. 12. Phonon band structures for the most relevant predicted modifications of CaZnOS: a) CaZnOS-*exp* type; b) 2H polytype; c) 4H polytype; d) 8H polytype; e)12R polytype. The calculations were performed using the hybrid HSE06 functional. Note that the labels of the special points correspond to a hexagonal (*hcp*) lattice.

In the case of the calculated and predicted CaZnOS crystal structures, we found that the CaZnOS-*exp* modification shows no imaginary frequencies in the phonon spectrum, indicating a stable crystal structure also found as a global minimum and in the experimental observations (Fig. 12). The 2H and 4H polytypes also show stable phonon bands (positive frequencies), indicating thermodynamic stability and crystal structures possible to be observed in future experiments. On the other hand, the 8H polytype shows slight imaginary frequencies at the Γ and A points of the Brillouin zone, suggesting metastability (Fig. 12d), while the 12R polytype has higher values of imaginary frequencies at several special points of the the Brillouin zone, resulting in possible phase transitions or decomposition (Fig. 12e). In principle, one could conclude that with the increase in the size of the polytype in the CaZnOS, the system becomes more unstable and harder to synthesize.

3.3. *Electronic properties and band structures of CaZnOS polytypes*

To further investigate the electronic structure and properties of the calculated CaZnOS modifications, band-structure calculations were carried out using the hybrid HSE06 functional. In the case of the CaZnOS-*exp* modification, the most stable and lowest energy minimum (V1) is presented in the Fig. 13a, while other variants are shown in the supporting information (Fig. S13). The calculations were accomplished for the hexagonal (*hcp*) unit cell along the high-symmetry path A–L–M–Γ–A–H–K–Γ of the Brillouin zone, as defined in ref [119]. In the CaZnOS-*exp* type, a direct band gap at the Γ point was found (Fig. 13a), and in the other variants of CaZnOS-*exp* modification (V2-V6), a direct band gap at the Γ point; however, the conduction band is nearly flat (showing weak dispersion) along the Γ–A direction (Fig. S13). Because the energy difference between the CBM at Γ and nearby *k*-point A is so small, the structure could effectively support an indirect band gap with a very slight energy difference, previously found in the related ZnO/ZnS system[47, 52]. For the 2H polytype, only one possible band structure was computed, and we observe the same trend: a possible indirect band gap along the Γ–A direction of the Brillouin zone, with less dispersion of the VBM due to a smaller structure (Fig. 13b).

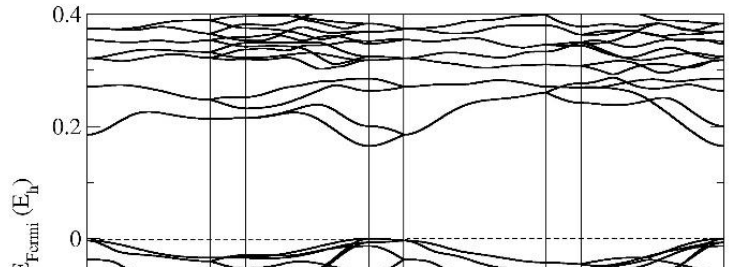

a)

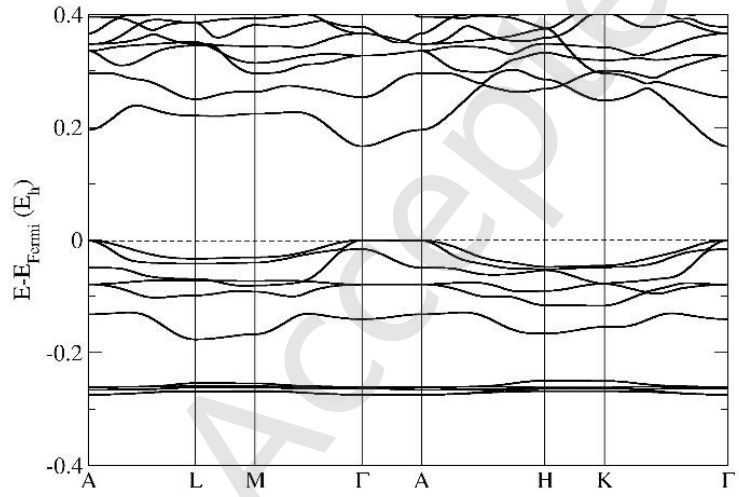

b)

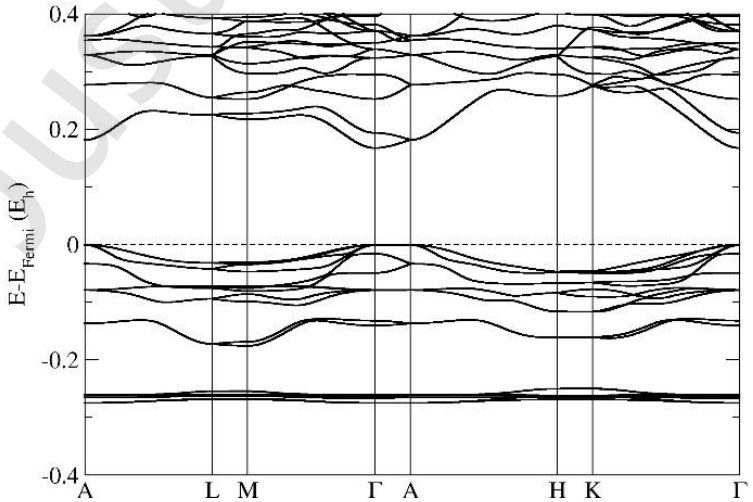

c)

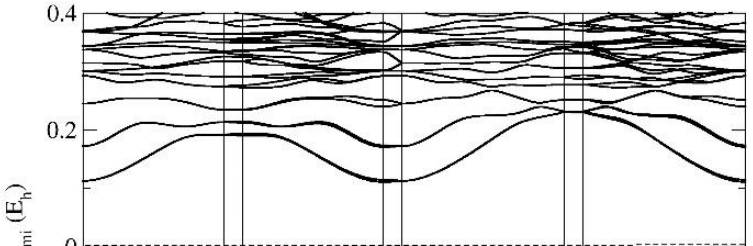

d)

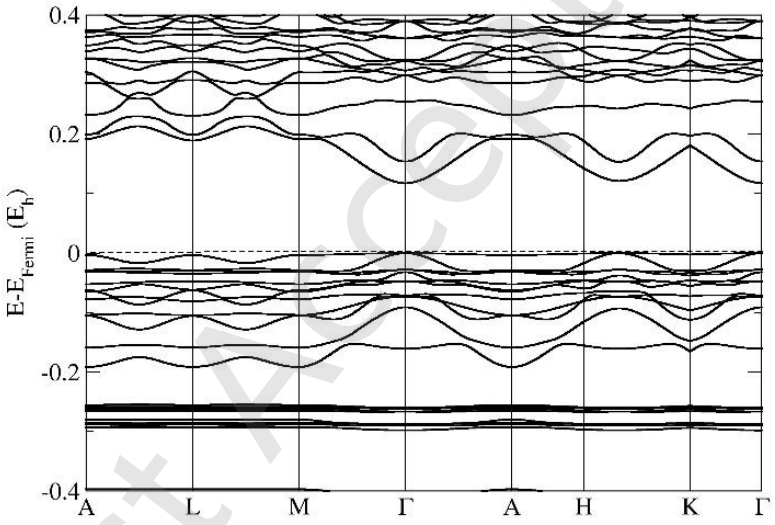

e)

Fig. 13. Band structure calculations for the most relevant predicted polytypic structures in CaZnOS: a) CaZnOS-*exp* type; b) 2H polytype; c) 4H polytype; d) 8H polytype; e) 12R polytype. The calculations were performed using the hybrid HSE06 functional.

In the case of the 4H polytype in CaZnOS, the band structure is quite similar to the CaZnOS-*exp* type, with the slight difference that a possible indirect gap was found at CBM along the Γ–A direction in all variants (Figs. 13c and S14). For the 8H polytype and all variants, the same trend continues, with greater band dispersion due to the larger polytypic structure. With such a small energy gap along the Γ–A direction, the structure may effectively exhibit an indirect transition with a minimal energy offset. (Figs. 13d and S15). Finally, the band structures from 12R polytypes and variants were computed using the hybrid HSE06 approximation (Figs. 13e and S16). Here, a direct

band gap at the Γ point was found, and in the other variants of 12R polytype (V2-V6), a possibility for an indirect band gap was found along the H-K direction (Figs. 13e and S16). This is consistent with previous data on ZnO polytypes, in which the rhombohedral unit cell was converted to a hexagonal unit cell for comparison. [42] The secondary band gap occurs along the H–K direction of the Brillouin zone, instead of at the A point, as in those polytypes that are naturally occurring in the hexagonal unit cell, as found here in CaZnOS.

4. DISCUSSION

The exploration of potential CaZnOS modifications predicts a variety of structural arrangements beyond those currently established, especially polytypic structures appearing in associated compounds. For example, in the chemically and structurally related ZnO/ZnS system, polytypes are configurations made up of corner-linked layers of $Zn(O/S)_4$ tetrahedra arranged in numerous sequences similar to the dense arrangements of spheres. The symbols used to categorize these polytypes carry specific significance; for instance, the number 3 in the 3C polytype (known as sphalerite in ZnO or ZnS) indicates the three-layer periodicity of the *fcc*-like (ABC) arrangement, while the letter C signifies the crystal's cubic symmetry. [101, 120-125] The wurtzite polytype *ABAB*..., which follows the *hcp*-like stacking sequence, [38, 101, 102, 121, 126-128] is labeled as 2H, with 2 representing the two-layer stacking periodicity and H referring to hexagonal symmetry. This periodicity is doubled, tripled, and quadrupled in the 4H, 6H, and 8H polytypes.

The family of rhombohedral polytypes is designated R, such as 9R, 12R, and 21R [37, 41, 113, 131-136]. As the polytype number increases, the stacking sequences become more intricate. In the following, we have predicted possible polytypes of CaZnOS, starting from the 2H polytypic structure and increasing the number of atoms and layers to 4H, 8H, and 12R, ensuring that each Zn atom is replaced by a Ca atom in the computed unit cell, resulting in stoichiometric CaZnOS. The predicted CaZnOS polytypes represent a combination of new and known stacking sequences that differ from previously reported ZnO/ZnS polytypes in the specific distribution of Ca, Zn, O, and S atoms. Moreover, we have predicted several stacking variants, marked V1-V6, from specific polytypic structures, including 2H, 4H, 8H, and 12R, as well as the CaZnOS exp modification. In this work, we did not attempt the experimental synthesis of 2H, 4H, 8H, and 12R polytype CaZnOS, since their experimental preparation can be challenging due to the possible metastability of the structures and the need for precise control of the synthesis conditions; however, the present study expands the understanding of oxychalcogenide polytypism and contributes to the literature with new variants of CaZnOS.

Although CaZnOS has been reported in the literature, this experimental study provides a detailed structural and quantitative analysis of the synthesized sample. Specifically: a Rietveld analysis based on the ICSD model was performed (#250092), [99] obtained lattice parameters (a = 3.7570(2) Å, c = 11.3968(9) Å) and refined atomic positions are in excellent agreement with the literature, [98, 99, 114] quantitative phase analysis was carried out, which shows ~85.9% CaZnOS and ~14.1% CaO, secondary phases were identified and analyzed, which enables a realistic

assessment of the quality of the sample. Our synthesis approach (solid-phase reaction in an inert Ar atmosphere at 1000 °C with controlled sulfur loss) provides an optimized protocol that ensures high phase purity and good crystal order, as evidenced by literature data [27-30, 98, 99, 114].

The presence of CaZnOS and CaO phases, identified by Rietveld analysis, indicates that the sample is a two-phase polycrystalline system rather than a single-phase material. Based on the XRPD data, the existence of coherent growth or epitaxial interaction between CaZnOS and CaO cannot be confirmed, so it is most likely that both phases exist as separate crystallites within a heterogeneous polycrystalline microstructure, resulting from a locally incomplete reaction and a complex balance of oxygen and sulfur during the synthesis in the solid phase.

CaZnOS is the dominant phase (~85.9%) and exhibits a well-defined, stable crystal structure under the given synthesis conditions, whereas CaO is a secondary phase arising from incomplete reaction or local thermodynamic conditions during the process. The complete isolation of the pure CaZnOS phase under identical synthesis conditions is difficult because oxide phases form competitively in the calcium-containing system at high temperatures. Nevertheless, the material obtained has a sufficiently high proportion of the main phase to enable reliable structural analysis and comparison with theoretical predictions.

Thus, the present experimental results confirm that the basic CaZnOS structure type ($P6_3mc$) is stable under realistic synthesis conditions, a crucial consideration for interpreting theoretically predicted alternative polytypes. Also, a detailed analysis of atomic positions and coordination (tetrahedral Zn and octahedral Ca environments) gives additional insight into the structural flexibility of the system, which is directly related to the possibility of forming different polytypes and doping. The CaZnOS exhibits significant structural flexibility, providing favorable sites for chemical substitution at the octahedral Ca^{2+} and tetrahedral Zn^{2+} sites, without major lattice distortion [28]. This ability to accommodate a wide range of dopant ions enables systematic tailoring of the material's optical, electronic, and catalytic properties, making it a versatile, multifunctional platform. Moreover, the hybrid oxide-sulfide composition of CaZnOS provides excellent thermal and chemical stability, enabling it to maintain strong luminescence even at elevated temperatures, a key requirement for LED and display applications.

A structure-property relationship outlines how the configuration of atoms, molecules, or materials determines their physical, chemical, and functional properties. This fundamental concept in chemistry, materials science, and biology enables the prediction and creation of materials with desired behaviors. Minor structural alterations, ranging from molecular arrangements and bonding to crystal sizes and processing techniques, can lead to significant differences in properties, laying the foundation for the development of novel materials and technologies.

The formation energies of all predicted polytypes and variants of CaZnOS were computed using the hybrid HSE06 functional (Table 8). All structures exhibit negative formation energies, indicating stability, in agreement with the computed *E(V)* curves (Figs. 11 and S7-S10). Such negative formation energies only indicate stability relative to constituent elements, not against decomposition into competing Ca–Zn–O–S phases. Consistent, OQMD-aligned calculations were performed to determine the formation energies and stabilities of various alternative CaZnOS polymorphs, with the results, phase diagram, and stability analysis added to the supporting

information (Figs. S11 and S12). We note that there are many competing phases on the CaZnOS phase diagram, and their relative stabilities are shown in the Ca-O-S-Zn phase diagram (Fig. S11). According to additional OQMD calculations using the quickhull algorithm for convex hulls, many elemental, binary, ternary, and quaternary systems have energies above the convex hull across various polymorphs (Fig. S11). [129, 130] All predicted CaZnOS structures on the phase diagram exhibit negative formation energies, which aligns with the present LCAO hybrid HSE06 calculations (Fig. S12). Thus, these negative values indicate baseline thermodynamic stability relative to the constituent elements.

Regarding the calculated CaZnOS polytypic structures, the experimental (CaZnOS-*exp*) modification exhibits no imaginary frequencies in its phonon spectrum. This confirms its dynamical stability as a global energy minimum, which is consistent with experimental observations. While the 2H and 4H polytypes exhibit purely positive frequencies, confirming their dynamical stability, the 8H and 12R polytypes display soft modes with imaginary frequencies, suggesting a tendency toward spontaneous lattice distortion and dynamical instability. The presence of three zero-frequency acoustic modes at the Γ point could indicate possible dynamical stability of the predicted 8H and 12R polytypes. On the other hand, acoustic modes at Γ are necessary but not sufficient to establish dynamical stability across the Brillouin zone. These polytypes exhibit dynamical instabilities in their bulk form at 0 K, and perhaps may be accessible via epitaxial strain, substrate effects, doping, or external pressure. [131-136]

This trend confirms that with increasing complexity of the polytype, structural instability increases, which is consistent with the strengthening of geometric distortions due to the mismatch of the ionic radii of Ca^{2+} (~1.00 Å, CN=6) and Zn^{2+} (~0.74 Å, CN=4) within the framework of mixed O/S coordination. [137] In this context, electronic effects can be seen as a secondary factor that further modifies local energy stability through charge redistribution between the O and S sublattices, but they do not constitute the primary mechanism of symmetry breaking. Instead, the primary cause remains ionic (radius mismatch Ca^{2+}/Zn^{2+}), while the electronic structure only reflects and locally stabilizes already existing geometric distortions, which is also consistent with the observed phonon behavior.

This theoretical study illustrates the wide range of structural features and band-gap values achievable in CaZnOS polytypic structures. Summary of all computed structural data (unit cell parameters) and band gap value for the most relevant polytypes in CaZnOS are shown in Table S1 and Fig. 14. The calculations in the present study were performed using the GGA-PBE, LDA-PZ, hybrid HSE06, B3LYP, and PBE0 functionals, and compared to previous experimental and theoretical results (Fig. 14). There is a good agreement between computed band gap for the experimentally observed CaZnOS-*exp* type in the range of 3.16-5.14 eV depending on the chosen functional (Table S1 and Fig. 14), compared to the previous experimental data with the band gap of 3.7 eV [98], as well as with previous GGA-PBE calculations of 3.90 eV [100]. Present DFT results agree even better with present experimental data of the cell parameters, where a = 3.7570(2) Å; c = 11.3968(9) Å, or previously reported XRD values of a = 3.75726(3) Å, c = 11.4013(1) Å [98], and a = 3.7547(1) Å, c = 11.4014(5) Å [99] (Fig. 14). We would like to point out that there is no previous literature data on the other polytypes of CaZnOS.

Upon examining the structure-property relationship, we identified several significant aspects of CaZnOS materials: potential structural distortions that result in reduced symmetry and/or phase transformation, which, on the other hand, influence the size of the unit cell, especially in the c direction of the unit cell, and computed band gap (Fig. 14). Thus, all calculations show that the 4H polytype has a slightly increased unit cell and band gap size compared to the CaZnOS experimentally observed polytype (Table S1 and Fig. 14).

Similarly, the band gap of the 2H polytype is slightly higher than that of the CaZnOS-*exp* type, regardless of the computational approach, but the symmetry is reduced, and the unit cell is twice as small, which might reduce costs in new technologies based on the 2H polytype. On the other side, the 8H polytype is twice as big as the CaZnOS-*exp* type, but has the same symmetry and the lowest possible band gap of all computed polytypes. However, the 8H polytype is a metastable structure that, if synthesized, could be used for band-gap tuning, perhaps via the transition route to the 4H polytype. The 12R polytype has the largest unit cell, rhombohedral symmetry, and a band gap between the experimental CaZnOS type and the 8H polytype, but it is highly unstable and would be very difficult to synthesize. We note that increasing the polytype size can significantly reduce the band gap and structural stability.

a)

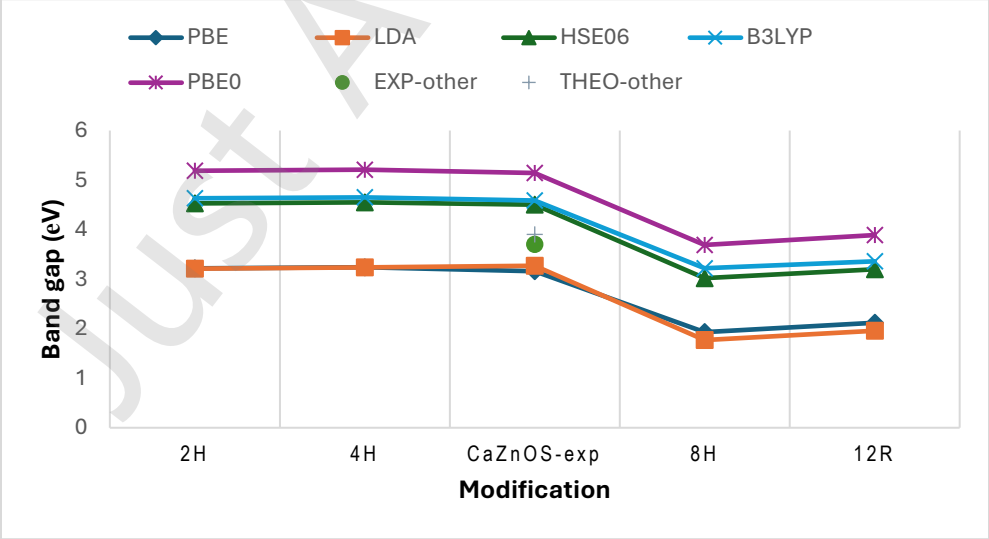

b)

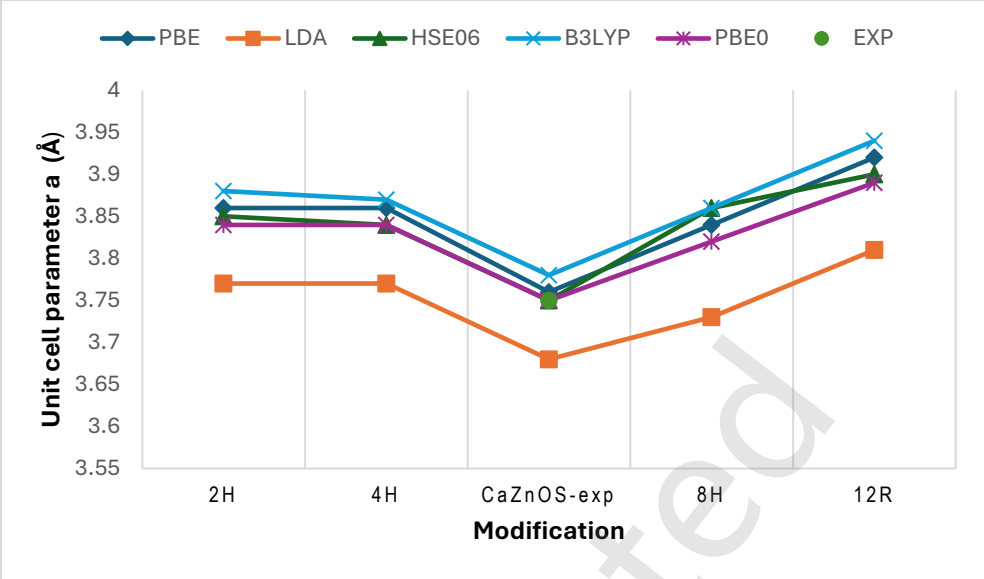

c)

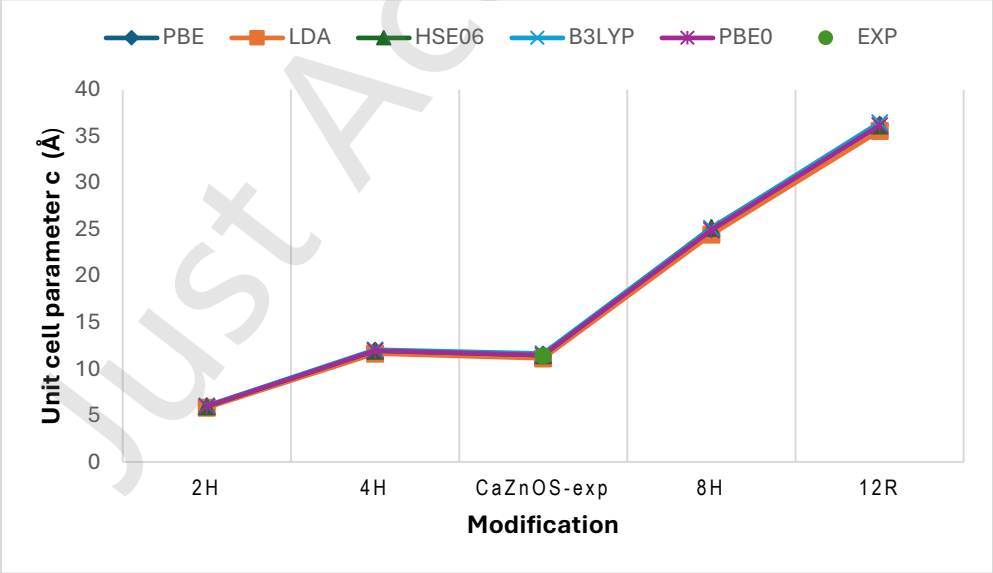

Fig. 14. Computed band gap size (a), and calculated structural data unit cell parameters *a* (b) and *c* (c) for the most relevant polytypic structures in CaZnOS. Present calculations were performed using the GGA-PBE, LDA-PZ, hybrid HSE06, B3LYP, and PBE0 functionals and were compared with previous experimental and theoretical data, when available.

Moreover, we note that the result with the LDA-PZ and GGA-PBE functionals show the smallest size of the band gap, while hybrid PBE0 show the highest values of the band gap regardless of the calculated polytype (Fig. 14a). When comparing the results of the computed unit cell parametres, we found that the LDA gives the smallest unit cell a parameter, while hybrid B3LYP gives the highest a parameter for any calculted CaZnOS polytype (Fig. 14b). In the case of the c direction of the unit cell, each of the five chosen functional (LDA-PZ, GGA-PBE, HSE06, B3LYP and PBE0) give similar results regardless of the calculated polytype (Fig. 14c).

5. CONCLUSION

The CaZnOS compound was investigated using a multidisciplinary approach combining experimental and theoretical methods, a strategy that has proven effective in previous studies. CaZnOS has been synthesized by a solid-state reaction in an inert argon atmosphere at 1000 °C. The crystal polytypic structure of CaZnOS was characterized by XRPD and appears in the hexagonal space group $P6_3mc$ (no.186). Structure prediction of new CaZnOS polytypes, including 2H, 4H, 8H, and 12R polytypes and their variations, was generated using recently developed PCAE and KOVIN algorithms, resulting in novel structural arrangements not reported previously for CaZnOS.

Ab initio calculations were performed using DFT with five functionals: LDA−PZ, GGA−PBE, B3LYP, PBE0, and HSE06. Full structural relaxation was performed for all predicted and calculated structures. When comparing computed structural data with the experimentally observed CaZnOS structure type, the best agreement was found with the hybrid HSE06 functional. Accordingly, the *E(V)* curves and phonon band structures were computed using the HSE06 functional in order to investigate the kinetic and thermodynamic stability of the structures. Moreover, for each polytype and several possible variants, the size of the optical band gap was computed, and the corresponding band structure. Finally, the most stable and relevant polytypic structures were investigated for structure-property relationships using five different functionals.

By analyzing the structure-property relationship, we discovered several key features of CaZnOS materials: possible structural deformations leading to reduced symmetry and/or phase changes, which, in turn, affect the unit cell dimensions and the calculated band gap. This study presents various potential stable and metastable CaZnOS polytypes within the specific layered CaZnOS polytypic structure, opening new possibilities for synthesis with specific opto-electronic and luminescent applications.

Acknowledgments:

The authors are grateful to R. Dovesi, K. Doll, and Crystal Solutions for software support with the CRYSTAL code. Furthermore, the authors acknowledge the support of the Center of Advanced Computing and Modelling at the University of Rijeka for providing computing resources. This

work was fully supported by the University of Rijeka under the research grant uniri-mz-25-28, funded by the European Union – NextGenerationEU, and by the Ministry of Science, Technological Development, and Innovation of the Republic of Serbia through based on Contract no. 451-03-136/2025-03/200017 ("Vinča" Institute of Nuclear Sciences - National Institute of the Republic of Serbia, University of Belgrade).

References

[1] Y. Li, M. Gecevicius, J. Qiu, Long persistent phosphors—from fundamentals to applications, Chemical Society Reviews, 45 (2016) 2090-2136.
[2] T. Matsuzawa, Y. Aoki, N. Takeuchi, Y. Murayama, A New Long Phosphorescent Phosphor with High Brightness, SrAl2 O 4 : Eu2 + , Dy3 + Journal of The Electrochemical Society, 143 (1996) 2670.
[3] T. Sharma, G. Arora, C.Y. Ng, H.K. Jun, A short review on long persistent luminescence materials and their application prospects in emerging photovoltaic devices, Heliyon, 10 (2024) e40341.
[4] V. Vitola, D. Millers, I. Bite, K. Smits, A. Spustaka, Recent progress in understanding the persistent luminescence in SrAl2O4:Eu,Dy, Materials Science and Technology, 35 (2019) 1661-1677.
[5] J.J. Joos, K. Korthout, L. Amidani, P. Glatzel, D. Poelman, P.F. Smet, Identification of Dy3+/Dy2+ as Electron Trap in Persistent Phosphors, Physical Review Letters, 125 (2020) 033001.
[6] J. Duan, J. Wang, Q. Tang, B. He, W. Wang, Long persistence phosphor assisted all-weather solar cells. Electricity generation beyond sunny days, Chemical Communications, 53 (2017) 3209-3212.
[7] Z. Tao, G. Hong, C. Shinji, C. Chen, S. Diao, A.L. Antaris, B. Zhang, Y. Zou, H. Dai, Biological Imaging Using Nanoparticles of Small Organic Molecules with Fluorescence Emission at Wavelengths Longer than 1000 nm, Angewandte Chemie International Edition, 52 (2013) 13002-13006.
[8] Z. Li, L. Huang, Y. Zhang, Y. Zhao, H. Yang, G. Han, Near-infrared light activated persistent luminescence nanoparticles via upconversion, Nano Research, 10 (2017) 1840-1846.
[9] K.S. Ahmad, S.B. Jaffri, J.S. Al-Hawadi, B. Makawana, R.K. Gupta, G.A. Ashraf, A.A.A. Bahajjaj, BaS3:Sb2S3:GdS2 Longitudinal Rods: Single-Source Precursor Synthesis, Characterization, and Electrochemical Applications for Supercapacitance and Catalysis, ChemistrySelect, 9 (2024) e202403344.
[10] L. Liang, N. Chen, Y. Jia, Q. Ma, J. Wang, Q. Yuan, W. Tan, Recent progress in engineering near-infrared persistent luminescence nanoprobes for time-resolved biosensing/bioimaging, Nano Research, 12 (2019) 1279-1292.
[11] N. Ullal, B. Sahoo, D. Sunil, S.D. Kulkarni, U. Bhat K, A. P.J, A. Rao, Ink formulations using Eu3+ doped strontium aluminates for security printing, Colloids and Surfaces A: Physicochemical and Engineering Aspects, 720 (2025) 137081.
[12] Kiran, Y. Dwivedi, Spectroscopic study of white light modulation in $SrAl_2O_4:Eu^{2+}$, Dy^{3+}-$ZnGa_2O_4:Cr^{3+}$ composite, Journal of Molecular Structure, 1341 (2025) 142645.
[13] B. Budde, H. Luo, P. Dorenbos, E. van der Kolk, Luminescent properties and energy level structure of CaZnOS:Eu2+, Optical Materials, 69 (2017) 378-381.
[14] Q.a. Chen, Z. Zhang, G. Xiong, L. Wang, The effect of different pigment on the adhesion mechanism of marine bacteria and Naviclua tenera on fluorescent antifouling coating, Surfaces and Interfaces, 60 (2025) 106061.

[15] R.-J. Xie, H.T. Hintzen, Optical Properties of (Oxy)Nitride Materials: A Review, Journal of the American Ceramic Society, 96 (2013) 665-687.
[16] P.F. Smet, J. Botterman, K. Van den Eeckhout, K. Korthout, D. Poelman, Persistent luminescence in nitride and oxynitride phosphors: A review, Optical Materials, 36 (2014) 1913-1919.
[17] A. Nande, S. Raut, S.J. Dhoble, Charge Transfer in Rare-Earth-Doped Inorganic Materials, in: V. Kumar, V. Sharma, H.C. Swart (Eds.) Advanced Materials for Solid State Lighting, Springer Nature Singapore, Singapore, 2023, pp. 31-58.
[18] D.A. Akulov, M.O. Kalinkin, R.M. Abashev, A.I. Surdo, N.I. Medvedeva, D.G. Kellerman, Rare-earth-doped fluorophosphate Li9Mg3[PO4]4F3 as a new material for dosimetric application, Journal of Alloys and Compounds, 1040 (2025) 183451.
[19] G. Chen, M. Zhu, D. Zhong, J. Liu, Y. Li, Y. Zang, S. Sun, H. Liu, S. Wang, Y. Xin, X. Wang, C. Hu, B. Teng, Transparent and Thermally Stable Rare-Earth-Doped Luminescent Gallate Glass toward Passive Daytime Radiative Cooling Applications, Inorganic Chemistry, 63 (2024) 21507-21518.
[20] T.B. Bekker, A.A. Ryadun, A.V. Davydov, V.P. Solntsev, V.D. Grigorieva, Luminescence properties of rare-earth-doped fluoride borate crystals, Journal of Alloys and Compounds, 900 (2022) 163343.
[21] S.N. Waithira, S. Kiprotich, A.H. Wako, G.S. Nyamato, Effects of pH on the Structural and Optical Properties of CaAl2O4: Eu2+, Dy3+ Nanoparticles, Trends in Sciences, 21 (2024) 8432.
[22] H. Ratinen, X-ray-excited optical fluorescence of ten rare earth ions in Y2O2S, La2O2S, and Gd2O2S, physica status solidi (a), 12 (1972) 447-451.
[23] Y. He, Y. Wu, R. Li, L. Wang, J. Zhang, X. Zhao, L. Shao, J. Pei, Innovative preparation of SrAl2O4:Eu2+, Dy3+ coatings for durable luminescent road markings, Case Studies in Construction Materials, 22 (2025) e04532.
[24] M.M. Islam, A Thorough Examination of Photocatalysis for Addressing Wastewater Pollution, ChemistrySelect, 10 (2025) e202500274.
[25] Y. Katayama, H. Kobayashi, J. Ueda, B. Viana, S. Tanabe, Persistent luminescence properties of Cr3+-Sm3+ activated LaAlO3 perovskite, Opt. Mater. Express, 6 (2016) 1500-1505.
[26] Z. Wang, X. Hou, Y. Liu, Z. Hui, Z. Huang, M. Fang, X. Wu, Luminescence properties and energy transfer behavior of colour-tunable white-emitting Sr4Al14O25 phosphors with co-doping of Eu2+, Eu3+ and Mn4+, RSC Advances, 7 (2017) 52995-53001.
[27] Y. Du, Y. Jiang, T. Sun, J. Zhao, B. Huang, D. Peng, F. Wang, Mechanically Excited Multicolor Luminescence in Lanthanide Ions, Advanced Materials, 31 (2019) 1807062.
[28] X. Zhang, H. Suo, Y. Wang, B. Chen, W. Zheng, Q. Wang, Y. Wang, Z. Zeng, S.-W. Tsang, D. Tu, F. Wang, Systematic Tuning of Persistent Luminescence in a Quaternary Wurtzite Crystal Through Synergistic Defect Engineering, Laser & Photonics Reviews, 17 (2023) 2300132.
[29] Z. Qiu, C. Rong, W. Zhou, J. Zhang, C. Li, L. Yu, S. Liu, S. Lian, A Strategy for Synthesizing CaZnOS:Eu2+ Phosphor and Comparison of Optical Properties with CaS:Eu2+, Journal of Alloys and Compounds, 583 (2014) 335-339.
[30] P.C. Ricci, J. Satta, D. Chiriu, R. Corpino, C.M. Carbonaro, M. Salis, C. Melis, P.S. Normile, J.A. De Toro, Optical and vibrational properties of CaZnOS: The role of intrinsic defects, Journal of Alloys and Compounds, 777 (2019) 225-233.
[31] U. Müller, Inorganic Structural Chemistry, Wiley-VCH, Marburg, Germany, 2007.
[32] F. Boutaiba, A. Belabbes, M. Ferhat, F. Bechstedt, Polytypism in ZnS, ZnSe, and ZnTe: First-principles study, Physical Review B, 89 (2014) 245308.
[33] S.M. Aksenov, D.O. Charkin, A.M. Banaru, D.A. Banaru, S.N. Volkov, D.V. Deineko, A.N. Kuznetsov, R.K. Rastsvetaeva, N.V. Chukanov, B.B. Shkurskii, N.A. Yamnova, Modularity, poly-typism, topology, and complexity of crystal structures of inorganic compounds (Review), Journal of Structural Chemistry, 64 (2023) 1797-2028.

[34] U.P. Tyagi, A. Saxena, M. Sharma, A systematic study of polytypism in melt & solution grown crystals of cadmium iodide doped with anionic & cationic impurities, Journal of Theoretical and Applied Physics, 19 (2025).
[35] M.M. Alsardia, I.B. Khadka, B. Ul Haq, S.H. Kim, First-Principles Investigations of the Physical Properties of Experimentally Feasible Novel Aluminum Nitride Polytypes, Crystal Growth and Design, 22 (2022) 2342-2353.
[36] H. Liang, Y. Zeng, L. Liu, J. Pu, H. Luo, Z. Xiong, W. Zhang, Z. Niu, L. Fang, Y. Zou, Polymorphism in Type-II Dirac Semimetal WSi2 under Pressure: Structural, Mechanical, and Electronic Insights, Inorganic Chemistry, 63 (2024) 22227-22238.
[37] S. Mardix, Polytypism: A controlled thermodynamic phenomenon, Physical Review B, 33 (1986) 8677-8684.
[38] Ü. Özgür, Y.I. Alivov, C. Liu, A. Teke, M.A. Reshchikov, S. Doğan, V. Avrutin, J.H. Cho, H. Morkoç, A comprehensive review of ZnO materials and devices, Journal of Applied Physics, 98 (2005) 041301.
[39] D. Fischer, D. Zagorac, J.C. Schön, The presence of superoxide ions and related dioxygen species in zinc oxide—A structural characterization by in situ Raman spectroscopy, J. Raman Spectrosc., 53 (2022) 2137-2146.
[40] S. Kumar, F. Fossard, G. Amiri, J.-M. Chauveau, V. Sallet, Induced structural modifications in ZnS nanowires via physical state of catalyst: Highlights of 15R crystal phase, Nano Research, 15 (2022) 377-385.
[41] M. Fonović, J. Zagorac, M. Čebela, D. Jordanov, D. Zagorac, Discovery of a new zinc oxide semiconductor: 21R polytype, Structural Dynamics, 12 (2025).
[42] D. Zagorac, J.C. Schön, J. Zagorac, M. Jansen, Theoretical investigations of novel zinc oxide polytypes and in-depth study of their electronic properties, RSC Advances, 5 (2015) 25929-25935.
[43] A. Menad, M.E. Benmalti, A. Zaoui, M. Ferhat, Impact of polytypism on the ground state properties of zinc oxide: A first-principles study, Results in Physics, 18 (2020) 103316.
[44] A. Apaolaza, D. Richard, M.R. Tejerina, Experimental and ab initio study of the structural and optical properties of ZnO coatings: Performance of the DFT+U approach, Processing and Application of Ceramics, 14 (2020) 362-371.
[45] M. Zafar, S. Ahmed, M. Shakil, M.A. Choudhary, First-principles calculations of structural, electronic, and thermodynamic properties of ZnO 1− x S x alloys, Chinese Physics B, 23 (2014) 106108.
[46] D. Zagorac, J. Zagorac, J.C. Schön, N. Stojanovic, B. Matovic, ZnO/ZnS (hetero)structures: ab initio investigations of polytypic behavior of mixed ZnO and ZnS compounds, Acta Crystallographica B, 74 (2018) 628-642.
[47] D. Zagorac, J. Zagorac, M. Pejić, B. Matović, J.C. Schön, Band Gap Engineering of Newly Discovered ZnO/ZnS Polytypic Nanomaterials, Nanomaterials, 12 (2022) 1595.
[48] S. Shabbir, A. Shaari, R. Ahmed, B. Ul Haq, S.-H. Kim, S. AlFaify, M. Anjum Javed, R. Ashraf, Physical properties of different polymorphs of sulfur doped ZnO studied in the framework of first-principles approaches, Materials Science and Engineering: B, 299 (2024) 116974.
[49] A. Tiwari, S. Bishnoi, S.J. Dhoble, Engineering ZnS nanoarchitectures: Defects and dynamic surfaces for improved photocatalysis, Journal of Molecular Structure, 1349 (2026).
[50] F. Mollaamin, M. Monajjemi, Designing of Zinc Oxide/Zinc Sulfide Heterojunction Arrays as Potential Semiconductors for Promoting Safe Energy Storage in Eco-Friendly Batteries, Energy Storage, 7 (2025).
[51] M. Ahmad, M. Ali, N.U. Islam, H. Ullah, K.F. Faway, X. Yi, M. Ikram, N. Zada, D. Shit, K. Jayabalan, Important features, applications and future perspective of zinc oxide based reduce graphene oxide nanocomposite, Reviews in Inorganic Chemistry, (2025).

[52] J. Zagorac, D. Zagorac, V. Šrot, M. Ranđelović, M. Pejić, P.A. van Aken, B. Matović, J.C. Schön, Synthesis, Characterization, and Electronic Properties of ZnO/ZnS Core/Shell Nanostructures Investigated Using a Multidisciplinary Approach, Materials, 16 (2023) 326.
[53] M. Čebela, P. Šenjug, D. Zagorac, I. Popov, J. Zagorac, M. Rosić, D. Pajić, Synthesis, Structural and Magnetic Properties of BiFeO3 Substituted with Ag, Materials, 18 (2025).
[54] D. Zagorac, M. Fonović, S. Butulija, A. Luković, V. Maksimović, J. Zagorac, B. Matović, A multi-disciplinary study of yttrium effect on the electronic structure of hafnia, Journal of Alloys and Compounds, 1010 (2025).
[55] J.C. Schön, Energy landscapes in inorganic chemistry, Comprehensive Inorganic Chemistry III, Third Edition2023, pp. 262-392.
[56] D. Zagorac, J.C. Schön, Energy landscapes of pure and doped ZnO: from bulk crystals to nanostructures, in: D. Wales (Ed.) Energy Landscapes of Nanoscale Systems, Elsevier2022.
[57] J.C. Schön, Energy landscapes—Past, present, and future: A perspective, The Journal of Chemical Physics, 161 (2024).
[58] K.P. Hilleke, T. Bi, E. Zurek, Materials under high pressure: a chemical perspective, Applied Physics A, 128 (2022) 441.
[59] J.C. Schön, Energy Landscape Concepts for Chemical Systems under Extreme Conditions, Journal of Innovative Materials in Extreme Conditions 2(2021) 5-57.
[60] T. Škundrić, D. Zagorac, J.C. Schön, M. Pejić, B. Matović, Crystal Structure Prediction of the Novel Cr2SiN4 Compound via Global Optimization, Data Mining, and the PCAE Method, Crystals, 11 (2021) 891.
[61] T. Hahn, International Tables for Crystallography, Volume A: Space-Group Symmetry, Springer Netherlands, Netherlands, 1992.
[62] D. Zagorac, C. Buyer, J. Zagorac, T. Škundrić, J.C. Schön, T. Schleid, Band-Gap Engineering and Unusual Behavior of Electronic Properties during Anion Substitution of Sulfur in LaFSe, Crystal Growth & Design, 24 (2024) 1648-1657.
[63] D.T. Teppala, M. Pejić, D. Zagorac, E. Adabifiroozjaei, N. Goyal, L. Molina-Luna, S. Mathur, B. Matović, E. Ionescu, Single-source precursor synthesis of a compositionally complex early transitional metal nitride (V, Nb, Ta, Mo, W)Nx and its high temperature stability, International Journal of Applied Ceramic Technology, 23 (2026) e70120.
[64] T. Škundrić, J.C. Schön, J. Zagorac, M. Pejić, D. Zagorac, Unveiling crystalline modifications on the energy landscape of Cr3Si3N8 using the multi-methodological approach, Computational and Theoretical Chemistry, 1256 (2026).
[65] B. Matović, N.M. Belozerova, D.P. Kozlenko, I.Y. Zel, J. Maletaškić, D. Zagorac, S. Butulija, I. Cvijović-Alagić, High-pressure behavior of high-entropy A2B2O7 pyrochlore, Ceramics International, 50 (2024) 52649-52654.
[66] R. Hundt, J.C. Schön, A. Hannemann, M. Jansen, Determination of symmetries and idealized cell parameters for simulated structures, Journal of Applied Crystallography, 32 (1999) 413-416.
[67] A. Hannemann, R. Hundt, J.C. Schön, M. Jansen, A New Algorithm for Space-Group Determination, Journal of Applied Crystallography, 31 (1998) 922-928.
[68] R. Hundt, J.C. Schön, M. Jansen, CMPZ - an algorithm for the efficient comparison of periodic structures, Journal of Applied Crystallography, 39 (2006) 6-16.
[69] R. Hundt, KPLOT: A Program for Plotting and Analysing Crystal Structures, Technicum Scientific Publishing, Stuttgart, 2016.
[70] K. Momma, F. Izumi, VESTA: a three-dimensional visualization system for electronic and structural analysis, Journal of Applied Crystallography, 41 (2008) 653-658.

[71] R. Dovesi, A. Erba, R. Orlando, C.M. Zicovich-Wilson, B. Civalleri, L. Maschio, M. Rérat, S. Casassa, J. Baima, S. Salustro, B. Kirtman, Quantum-mechanical condensed matter simulations with CRYSTAL, WIREs Computational Molecular Science, 8 (2018) e1360.
[72] R. Dovesi, F. Pascale, B. Civalleri, K. Doll, N.M. Harrison, I. Bush, P. D'Arco, Y. Noël, M. Rérat, P. Carbonnière, M. Causà, S. Salustro, V. Lacivita, B. Kirtman, A.M. Ferrari, F.S. Gentile, J. Baima, M. Ferrero, R. Demichelis, M.D.L. Pierre, The CRYSTAL code, 1976–2020 and beyond, a long story, The Journal of Chemical Physics, 152 (2020) 204111.
[73] B. Civalleri, P. D'Arco, R. Orlando, V.R. Saunders, R. Dovesi, Hartree–Fock geometry optimisation of periodic systems with the Crystal code, Chemical Physics Letters, 348 (2001) 131-138.
[74] J.P. Perdew, K. Burke, M. Ernzerhof, Generalized Gradient Approximation Made Simple, Physical Review Letters, 77 (1996) 3865-3868.
[75] J.C. Slater, The Theory of Complex Spectra, Physical Review, 34 (1929) 1293-1322.
[76] J.C. Slater, The Self-Consistent Field for Molecular and Solids, Quantum Theory of Molecular and Solids, McGraw-Hill, New York, USA, 1974.
[77] J.P. Perdew, A. Zunger, Self-interaction correction to density-functional approximations for many-electron systems, Physical Review B, 23 (1981) 5048-5079.
[78] A.D. Becke, Density-functional thermochemistry. III. The role of exact exchange, The Journal of Chemical Physics, 98 (1993) 5648-5652.
[79] J. Heyd, G.E. Scuseria, M. Ernzerhof, Hybrid functionals based on a screened Coulomb potential, The Journal of Chemical Physics, 118 (2003) 8207-8215.
[80] J.P. Perdew, M. Ernzerhof, K. Burke, Rationale for mixing exact exchange with density functional approximations, The Journal of Chemical Physics, 105 (1996) 9982-9985.
[81] C. Adamo, V. Barone, Toward reliable density functional methods without adjustable parameters: The PBE0 model, The Journal of Chemical Physics, 110 (1999) 6158-6170.
[82] C. Buyer, H. Grossholz, S. Wolf, D. Zagorac, J. Zagorac, J.C. Schön, T. Schleid, Crystal-Structure Prediction and Experimental Investigation of the Polymorphic Lanthanum Fluoride Selenides LaFSe and La2F4Se, Crystal Growth & Design, 22 (2022) 7133-7142.
[83] J.C. Schön, Ž. Čančarević, M. Jansen, Structure prediction of high-pressure phases for alkali metal sulfides, The Journal of Chemical Physics, 121 (2004) 2289-2304.
[84] D. Zagorac, K. Doll, J. Zagorac, D. Jordanov, B. Matović, Barium Sulfide under Pressure: Discovery of Metastable Polymorphs and Investigation of Electronic Properties on ab Initio Level, Inorganic Chemistry, 56 (2017) 10644-10654.
[85] D. Zagorac, J.C. Schön, J. Zagorac, M. Jansen, Prediction of structure candidates for zinc oxide as a function of pressure and investigation of their electronic properties, Physical Review B, 89 (2014) 075201.
[86] J.E. Jaffe, A.C. Hess, Hartree-Fock study of phase changes in ZnO at high pressure, Physical Review B, 48 (1993) 7903-7909.
[87] T. Homann, U. Hotje, M. Binnewies, A. Börger, K.-D. Becker, T. Bredow, Composition-dependent band gap in $ZnS_xSe_{1-x:}$ a combined experimental and theoretical study, Solid State Sciences, 8 (2006) 44-49.
[88] M. Catti, A. Pavese, V.R. Saunders, Elastic constants and electronic structure of fluorite (CaF2): an ab initio Hartree-Fock study, Journal of Physics: Condensed Matter, 3 (1991) 4151.
[89] Tamara Škundrić, Branko Matović, Aleksandra Zarubica, Dorota Chudoba, D. Zagorac, Data mining ab initio study of gypsum and caco3 modifications at standard and extreme conditions, Journal of Innovative Materials in Extreme Conditions, 4 (2023) 38-51.
[90] M.D. Towler, N.L. Allan, N.M. Harrison, V.R. Saunders, W.C. Mackrodt, E. Aprà, Ab initio study of MnO and NiO, Physical Review B, 50 (1994) 5041-5054.

[91] A.M. Ferrari, C. Pisani, An ab Initio Periodic Study of NiO Supported at the Pd(100) Surface. Part 1: The Perfect Epitaxial Monolayer, The Journal of Physical Chemistry B, 110 (2006) 7909-7917.
[92] M. Mian, N.M. Harrison, V.R. Saunders, W.R. Flavell, An ab initio Hartree-Fock investigation of galena (PbS), Chemical Physics Letters, 257 (1996) 627-632.
[93] D. Zagorac, K. Doll, J.C. Schön, M. Jansen, Ab initio structure prediction for lead sulfide at standard and elevated pressures, Physical Review B, 84 (2011) 045206.
[94] F. Pascale, C.M. Zicovich-Wilson, F. López Gejo, B. Civalleri, R. Orlando, R. Dovesi, The calculation of the vibrational frequencies of crystalline compounds and its implementation in the CRYSTAL code, Journal of Computational Chemistry, 25 (2004) 888-897.
[95] D. Zagorac, K. Doll, J.C. Schön, M. Jansen, Sterically Active Electron Pairs in Lead Sulfide? An Investigation of the Electronic and Vibrational Properties of PbS in the Transition Region Between the Rock Salt and the α-GeTe-Type Modifications, Chemistry – A European Journal, 18 (2012) 10929-10936.
[96] D. Zagorac, H. Mueller, S. Ruehl, J. Zagorac, S. Rehme, Recent developments in the Inorganic Crystal Structure Database: theoretical crystal structure data and related features, J. Appl. Cryst., 52 (2019) 918-925.
[97] J. Rodríguez-Carvajal, Recent advances in magnetic structure determination by neutron powder diffraction, Physica B: Condensed Matter, 192 (1993) 55-69.
[98] T. Sambrook, C.F. Smura, S.J. Clarke, K.M. Ok, P.S. Halasyamani, Structure and Physical Properties of the Polar Oxysulfide CaZnOS, Inorganic Chemistry, 46 (2007) 2571-2574.
[99] S.A. Petrova, V.P. Mar'evich, R.G. Zakharov, E.N. Selivanov, V.M. Chumarev, L.Y. Udoeva, Crystal Structure of Zinc Calcium Oxysulfide, Doklady Chemistry, 393 (2003) 255-258.
[100] J. He, Z. Yao, V.I. Hegde, S.S. Naghavi, J. Shen, K.M. Bushick, C. Wolverton, Computational Discovery of Stable Heteroanionic Oxychalcogenides ABXO (A, B = Metals; X = S, Se, and Te) and Their Potential Applications, Chemistry of Materials, 32 (2020) 8229-8242.
[101] S.D. Scott, H.L. Barnes, Sphalerite-wurtzite equilibria and stoichiometry, Geochimica et Cosmochimica Acta, 36 (1972) 1275-1295.
[102] H. Sowa, H. Ahsbahs, High-pressure X-ray investigation of zincite ZnO single crystals using diamond anvils with an improved shape, Journal of Applied Crystallography, 39 (2006) 169-175.
[103] D. Fischer, D. Zagorac, J.C. Schön, Fundamental insight into the formation of the zinc oxide crystal structure, Thin Solid Films, 782 (2023) 140017.
[104] H. Suo, X. Zhang, F. Wang, Controlling X-ray-activated persistent luminescence for emerging applications, Trends in Chemistry, 4 (2022) 726-738.
[105] S. Mardix, I. Kiflawi, Z.H. Kalman, Double polytype regions in ZnS crystals, Acta Crystallographica Section B, 25 (1969) 1586-1589.
[106] Z. Huang, T.-Y. Lü, H.-Q. Wang, J.-C. Zheng, Thermoelectric properties of the 3C, 2H, 4H, and 6H polytypes of the wide-band-gap semiconductors SiC, GaN, and ZnO, AIP Advances, 5 (2015).
[107] S. Shabbir, A. Shaari, B. Ul Haq, R. Ahmed, S. AlFaify, M. Ahmed, A. Laref, First-principles investigations of electronic structures and optical spectra of wurtzite and sphalerite types of ZnO1-xSx (x=0, 0.25, 0.50, 0.75 &1) alloys, Materials Science in Semiconductor Processing, 121 (2021) 105326.
[108] R. Kapil, B.R. Mehta, V.D. Vankar, Growth of 8H polytype of diamond using cyclic growth/etch oxy-acetylene flame setup, Thin Solid Films, 312 (1998) 106-110.
[109] K. Kobayashi, S. Komatsu, First-Principles Study of 8H-, 10H-, 12H-, and 18H-SiC Polytypes, Journal of the Physical Society of Japan, 81 (2012) 024714.
[110] W. Paszkowicz, P. Dłużewski, Z.M. Spolnik, F. Firszt, H. Męczyńska, Formation of 4H and 8H polytypes in bulk Zn1−xMgxSe crystals, Journal of Alloys and Compounds, 286 (1999) 224-235.

[111] Y. Zhang, G. Li, F. Yuan, F. Han, M. Ali, W. Guo, J. Ren, Atomic scale observation of FCC twin, FCC → 9R and 9R → 12R' transformations in cold-rolled Hafnium, Scripta Materialia, 207 (2022) 114284.
[112] R. Batchelor, T. Birchall, Structure of cuprous iodide, polytype 12R, Acta Crystallographica Section B, 38 (1982) 1260-1263.
[113] H. Yang, Y.K. Tang, L.D. Yao, W. Zhang, Q.A. Li, F.Y. Li, C.Q. Jin, R.C. Yu, Synthesis, structure and phase separation of a new 12R-type perovskite-related oxide Ba3NdMn2O9, Journal of Alloys and Compounds, 432 (2007) 283-288.
[114] L. Guo, T. Li, C. Zhu, W. Liang, L. Wu, Tunable luminescent chromaticity of CaZnOS: Bi3+, Eu3+ with white emitting based on energy transfer, Journal of Alloys and Compounds, 905 (2022) 164262.
[115] J.E. Saal, S. Kirklin, M. Aykol, B. Meredig, C. Wolverton, Materials Design and Discovery with High-Throughput Density Functional Theory: The Open Quantum Materials Database (OQMD), JOM, 65 (2013) 1501-1509.
[116] S. Kirklin, J.E. Saal, B. Meredig, A. Thompson, J.W. Doak, M. Aykol, S. Rühl, C. Wolverton, The Open Quantum Materials Database (OQMD): assessing the accuracy of DFT formation energies, npj Computational Materials, 1 (2015) 15010.
[117] D. Zagorac, D.L.V.K. Prasad, T. Škundrić, K. Yadav, S. Singh, S. Laketić, J. Zagorac, M. Momčilović, I. Cvijović-Alagić, Mechanical properties and behavior of the Ti–45Nb alloy subjected to extreme conditions, CrystEngComm, 26 (2024) 2989-3004.
[118] B. Singh, M.K. Gupta, R. Mittal, S.L. Chaplot, Phonons, phase transitions and thermal expansion in LiAlO2: an ab initio density functional study, Physical Chemistry Chemical Physics, 20 (2018) 12248-12259.
[119] M.I. Aroyo, D. Orobengoa, G. de la Flor, E.S. Tasci, J.M. Perez-Mato, H. Wondratschek, Brillouin-zone database on the Bilbao Crystallographic Server, Acta Crystallographica Section A, 70 (2014) 126-137.
[120] W. Gerlach, Das Kα-Dublett, nebst einer Neubestimmung der Gitterkonstanten einiger Krystalle, Zeitschrift für Physik, 23 (1922) 114-120.
[121] A.F. Wells, Structural Inorganic Chemistry (5th ed.), Clarendon Press, Oxford, UK, 1984.
[122] M. Logar, B. Jančar, A. Rečnik, D. Suvorov, Controlled synthesis of pure and doped ZnS nanoparticles in weak polyion assemblies: growth characteristics and fluorescence properties, Nanotechnology, 20 (2009) 275601.
[123] S. Desgreniers, L. Beaulieu, I. Lepage, Pressure-induced structural changes in ZnS, Physical Review B, 61 (2000) 8726-8733.
[124] W.L. Bragg, J.A. Darbyshire, The structure of thin films of certain metallic oxides, Transactions of the Faraday Society, 28 (1932) 522-529.
[125] S.-K. Kim, S.-Y. Jeong, C.-R. Cho, Structural reconstruction of hexagonal to cubic ZnO films on Pt/Ti/SiO2/Si substrate by annealing, Applied Physics Letters, 82 (2003) 562-564.
[126] T. Suski, W. Paul, High Pressure in Semiconductor Physics I, Semiconductors and Semimetals, Academic Press, San Diego, 1998.
[127] E.H. Kisi, M.M. Elcombe, u parameters for the wurtzite structure of ZnS and ZnO using powder neutron diffraction, Acta Crystallographica Section C, 45 (1989) 1867-1870.
[128] M. Pejić, D.D. Zimmermann, D. Zagorac, M. Fonović, J. Zagorac, J.C. Schön, T. Schleid, Structural exploration of holmium fluoride selenide (HoFSe): theory and experiment, Journal of Physics and Chemistry of Solids, 208 (2026) 113000.
[129] C.B. Barber, D.P. Dobkin, H. Huhdanpaa, The quickhull algorithm for convex hulls, ACM Trans. Math. Softw., 22 (1996) 469–483.

[130] V. Stevanović, S. Lany, X. Zhang, A. Zunger, Correcting density functional theory for accurate predictions of compound enthalpies of formation: Fitted elemental-phase reference energies, Physical Review B, 85 (2012) 115104.
[131] Z.-J. Zhang, A. Feng, S.-L. Zhang, W.-B. Zhang, W. Yang, Mechanical properties of layered oxysulfide CaZnOS from first principle calculations, Journal of Alloys and Compounds, 670 (2016) 41-47.
[132] D. Fischer, D. Bloos, A. Krajewska, G.M. McNally, D. Zagorac, J.C. Schön, Raman Characterization of Dioxygen Species as Defects in Single-Crystal ZnO Including Their Pressure Dependence, Crystals, 15 (2025) 574.
[133] C. Larquet, S. Carenco, Metal Oxysulfides: From Bulk Compounds to Nanomaterials, Frontiers in Chemistry, 8 (2020).
[134] C. Murugan, S. Ramamoorthy, R.S. Ghuge, Y. Sivalingam, A. Sundaramurthy, Structure–Property Control through Sulfur Incorporation into Multicomponent Core–Shell Superstructures for the Detection of 1-Hexanol and Nonanal, ACS Applied Nano Materials, (2026).
[135] A. Gupta, A. Kumar, M.P. Srivastava, D.K. Rana, Facile Growth of Zinc Oxysulfide Nano Thin Film-based Visible Light Photosensor by Hydrothermal Method, ECS Journal of Solid State Science and Technology, 13 (2024).
[136] H. Althubyani, D. Stoeffler, J. Bartringer, S. Roques, D. Ihiawakrim, A. Dinia, T. Fix, Investigation of CaZrO3−xSx oxysulfide perovskite thin films grown by pulsed laser deposition, Journal of Physics: Energy, 8 (2026) 015034.
[137] R.D. Shannon, Revised effective ionic radii and systematic studies of interatomic distances in halides and chalcogenides, Acta Crystallographica Section A, 32 (1976) 751-767.